6-2004

Cold Flow Testing of a Modified Subscale Model Exhaust System for a Space Based Laser

David B. Jarrett

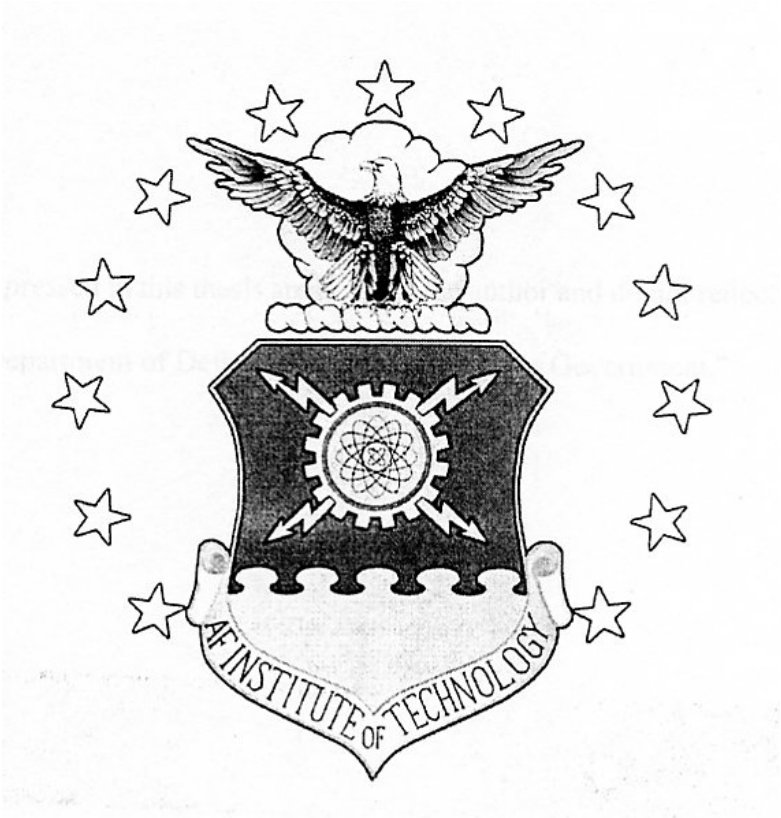

COLD FLOW TESTING OF A MODIFIED SUBSCALE MODEL EXHAUST SYSTEM FOR A SPACE BASED LASER

THESIS

David B. Jarrett, Ensign, USN
AFIT/GAE/ENY/04-J04

DEPARTMENT OF THE AIR FORCE
AIR UNIVERSITY

AIR FORCE INSTITUTE OF TECHNOLOGY

Wright-Patterson Air Force Base, Ohio

The views expressed in this thesis are those of the author and do not reflect the official policy or position of the United States Air Force, Department of Defense, or the United States Government.

AFIT/GAE/ENY/04-J04

COLD FLOW TESTING OF A MODIFIED SUBSCALE MODEL EXHAUST SYSTEM FOR A SPACE BASED LASER

THESIS

Presented to the Faculty

Department of Aeronautics and Astronautics

Graduate School of Engineering and Management

Air Force Institute of Technology

Air University

Air Education and Training Command

In Partial Fulfillment of the Requirements for the

Degree of Master of Science in Aeronautical Engineering

David B. Jarrett, BSME

Ensign, USN

June 2004

AFIT/GAE/ENY/04-J04

COLD FLOW TESTING OF A MODIFIED SUBSCALE MODEL EXHAUST SYSTEM FOR A SPACE BASED LASER

David B. Jarrett, BSME
Ensign, USN

Approved:

_____	_____
Milton E. Franke Ph.D. (Chairman)	date
_____	_____
Mark F. Reeder Ph.D. (Member)	date
_____	_____
Paul I. King Ph.D. (Member)	date

Abstract

The aim of this research was a continued study of gas-dynamic phenomena that occurred in a set of stacked nozzles as reported by Captains Ian Bautista in 2003 and Scott Bergren in 2002. The arrangement of the stacked nozzles was a modified version of a $1/5^{th}$ scale-model of one quadrant of the conceptual Space Based Laser Integrated Flight Experiment (SBL IFX) gas dynamic laser. Rather than cylindrical rings of nozzles, the stacked nozzles were flat and able to be rotated about a vector normal to the nozzle exits. This set of stacked flat nozzles was installed on a blow-down/vacuum wind tunnel, which in addition to the nozzles, consisted of a stilling chamber, centerbody, supersonic diffuser, and transition structure to join the vacuum and test sections.

The goals of this research were two fold; first, modify the original scale-model of the stacked cylindrical rings of nozzles so schlieren photography could be used to visualize an average flow field across the nozzles. Secondly, using the schlieren photographs, in conjunction with pressure data, observe the interactions between the individual nozzles. Results have shown that the modified nozzle array produces a vastly complex flow field as well as a highly supersonic flow régime, with Mach numbers that reach as high as 5.6.

Acknowledgments

I would like to extend a great deal of appreciation to my wife for her understanding and patients while I worked through many late nights. Secondly, I would like to thank my faculty advisor, Dr. Milton E. Franke, for his guidance and support. More often than not, the wisdom he shared shed light into an often-misunderstood subject. Additionally, I owe a great deal gratitude to Andy Pitts, the lab technician. Without his help the process of producing this thesis would have taken twice as long. Lastly, but by no means least, I would like to thank my shipmates for their help and support throughout the entire graduate education experience.

Table of Contents

Page

Page

List of Figures

Page

Page

List of Tables

Page

List of Symbols

Symbol	Definition	Units
English Notation		
A	Cross-sectional area perpendicular to flow	m^2
a	Acoustic velocity	m/s
D	Boundary layer thickness	m
M	Mach number	dimensionless
$\dot{m}$	Mass flow rate	kg/s
P	Pressure	Pa
R	Specific gas constant	J/kgK
Re	Reynolds number	dimensionless
T	Temperature	K
u	X-component of velocity	m/s
V	Velocity	m/s
w	Y-component of velocity	m/s
Greek Notation		
β	Oblique shock wave angle	deg
δ	Characteristic length (usually chord for flow over wing)	m
γ	Ratio of specific heats	dimensionless
μ	Viscosity	kg/(m s)
θ	Wedge half angle	deg
ρ	Density	kg/m^3
ν	Kinematic viscosity	m^2/s
Subscripts/Superscripts		
*	Critical dimension	
a	Atmospheric conditions	
n	Normal component	
ne	Nozzle exit conditions	
t	Total/Stagnation quantity (when used on pressure or temperature)	
t	Tangential component (when used on velocities or Mach number)	
1	Upstream location	
2	Downstream location	

COLD FLOW TESTING OF A MODIFIED SUBSCALE MODEL EXHAUST SYSTEM FOR A SPACE BASED LASER

I. Introduction

Background

From its inception in World War II, the Intercontinental Ballistic Missiles (ICBM) has been a major threat to the United States and its allies. Since that time, the U.S. has sought ways to counter the threat posed by an ICBM launched by an aggressive or rogue state. To that end, the Defense Advanced Research Projects Agency (DARPA), in conjunction with the Airborne Laser Laboratory, have studied the use of an Airborne Laser (ABL) to counter the ICBM threats. Preliminary tests conducted in the early 1970's through the 1980's yielded a Mid Infrared Advanced Chemical Laser (MIRACL) for use against airborne threats. This system was "*tested against tactical missiles and drone aircraft.*" (Federation, 2002) More recently the U. S. Air Force, the Ballistic Missile Defense Organization (BMDO), and an industry joint venture continue to evaluate the value of a Space Based Laser (SBL) for use against a ballistic missile threat in a program called the Space-Based Laser Integrated Flight Experiment (SBL IFX) (Possel, 1998). Today the U.S. Army in cooperation with the government of Israel have developed the Tactical High Energy Laser (THEL), with the specific objective of neutralizing theater ballistic missiles (Perram, 2004).

The SBL IFX planned to investigate the possibility of using a gas dynamic laser (GDL) in space, rather than on an airborne platform, with the objective of destroying ballistic missiles during their boost phase of flight (Bautista, 2003: 1-1). A hydrogen fluoride (HF) laser, powered

by an exothermic reaction of hydrogen and dissociated fluorine, was planned as the primary weapon for the SBL. However, this technology had to be proven before HF laser system can be implemented. The goal of the SBL IFX was to prove this technology by demonstrating the capability of the HF laser and by using integrated components of an SBL in a ground experiment via a demonstration of the high power elements of a space-based laser (Bautista, 2003: 1-2). Since then, it has become clear that the practicality of putting a laser in space and maintaining it is unfeasible. Rather than abandon the concept of using lasers as a counter to theater ballistic missiles, and lose the knowledge, the THEL program has studied the feasibility of using the same technology in a ground-based system.

Internal fluid dynamics are paramount to producing a GDL of sufficient power to be used in this application. It was therefore the purpose of this study to continue the work already completed in this area. As mentioned before, the hydrogen fluorine laser is powered by an exothermic reaction between hydrogen and dissociated fluorine. This exothermic reaction is accomplished by accelerating fluorine supersonically through an array of nozzles. In the divergent section of the nozzles, molecular hydrogen is injected to produce a well-mixed efficient reaction with the fluorine. The result is a vibrationally inverted HF molecule, which is required for the lasing process. Additionally, beam quality is also highly dependent on fluid flow properties within the lasing cavity. In a personal interview of Peter Lohn, conducted by Capt. Bautista, Mr. Lohn stated that low density, pressure, and temperature are all required for a high quality beam (Bautista, 2003: 1-2). Lowered density reduces the deactivation of excited HF molecules, lowered pressure promotes molecular diffusion, while low temperatures promotes laser inversion and ultimately higher gain. Shock waves and boundary layer separation cause

beam distortion, so simply high Mach number flow is not enough. What is truly desired in the lasing cavity is a high Mach number homogeneous fluid.

Problem Statement

It can now be seen that a high Mach number homogeneous fluid is ideal when developing a laser weapon. The crux of this design challenge is that to achieve a high Mach number with an array of nozzles; unfortunately, each nozzle produces its own shock diamond pattern encouraging beam distortion. Since these nozzles are in close proximity with each other, likewise so are the shock diamonds, the resultant flow field becomes a vastly complicated one. The big question that now arises is, "What does the shock pattern at the nozzle array exit look like, and how will it affect beam distortion?"

Objectives

The objectives of this research are two fold. First, design a nozzle array that will incorporate the same nozzle geometry as in the previous experiment and that can be used to observe the intricate interactions between individual nozzles. This objective was met with the use of a flat, rather than curved nozzle array. The new nozzle array would have a flat exit plane but would retain the original nozzle geometry; because of this change the total exit area would be reduced. In fact, the original $1/5^{th}$ scale nozzle array had an exit area of 11 cm^2, the new nozzle array only has 6.842 cm^2, a reduction of almost one half. This area reduction is due to the fact that the new nozzle array is flat vice curved like the $1/5^{th}$ scale model. Furthermore this new nozzle array is able to rotate about its base 360^O in 7.5^O increments. The second objective was to examine the flow field of the new nozzle array using time based pressure measurements and schlieren photographs. This objective was accomplished through the use of a basic schlieren

setup and a rapid data acquisition system collecting static pressure measurements at the same locations as in previous experiments.

Summary of Previous Work

Captain Scott Bergren initially, in 2002, conducted a study in which a $1/5^{th}$ –scale model of the nozzle rings and exhaust manifold from the SBL IFX were tested in a blow-down/vacuum wind tunnel. In this study it was found that the flow quality was very conducive to high beam quality. However, due to equipment limitations, the duration of the high quality flow only lasted for approximately 0.2 seconds. This short run time is only associated with the ground facilities and not indicative of space operations. Unfortunately, this duration time is too short for a very detailed study of the flow field (Bergren, 2002: xi).

Captain Ian Bautista continued Captain Bergren's work by investigating ways to increase the duration of the high quality flow field. This research produced a new transition structure which when used in the previous setup increased the flow duration from 0.2 seconds to approximately 10 seconds. Although the flow duration was increased the flow field quality did not decrease from what was previously attained (Bautista, 2003: xii).

Experimental Method

To accommodate the first objective, a new nozzle array was designed. With this new design came a few questions, they were:

1.) How much throat area will be lost and will it be small enough to be ignored?

2.) How much will the mass flow be affected?

3.) How will the new nozzle have to be designed to be able to achieve good images?

4.) How will the new nozzle array be mounted?

Once fabrication of the new nozzle was complete, the following general procedures were used to collect data and make conclusions about the flow field.

1.) Run the experiment with the nozzle array in the vertical position for the sake of comparison.
2.) Run the experiment with the nozzle array in the horizontal position, placing pressure transducers at key locations along the wind tunnel.
3.) Obtain schlieren images inside the optical cavity.
4.) Record wall static pressures at the transducer locations.
5.) Calculate mach numbers based on pressure readings and schlieren images
6.) Observe shock patterns via schlieren images.

This thesis is organized in such a manor that allows the reader to understand why particular design choices were incorporated into the test facility for the SBL IFX; in addition to the procedures and equipment that were used throughout the experimentation. The theory chapter will explain the fundamentals of compressible fluids and turbulent compressible jets, which is required to understand the flow field inside the lasing cavity.

The Procedural Methods chapter will elaborate on the procedure and equipment used. Additionally this chapter will discuss how one could duplicate the experiment to achieve the same results.

A Results chapter will present and discuss data collected. For ease of understanding to the reader, the majority of the presented results will be in the pictorial or tabulated form.

Finally, a Conclusions and Recommendations chapter will close this thesis by summarily explaining the relevance and applications for the findings documented in this study. Additionally, this chapter will suggest paths to future endeavors in this work in an effort to achieve more in-depth results by offering a few lessons learned.

II. Theory

Compressible Gas Dynamics

In the area of compressible gasses, the concept of quasi-one-dimensional flow is key, especially when considering supersonic nozzles. What differentiates quasi-one-dimensional flow from one-dimensional flow is that one-dimensional flow is considered to have a constant area, whereas quasi-one-dimensional flow allows the cross-sectional area to change in the direction of the flow. This can be graphically visualized as being the difference between flow through a straight pipe and flow through say a converging-diverging nozzle (Anderson, 1990: 147). Quasi-one-dimensional flow is the type of flow that was studied in the supersonic nozzle array.

The intrinsic properties of a thermally and calorically perfect gas, such as air, allow us to calculate the mass flow rate of that gas through a choked convergent nozzle. The relationship; found in equation 1 below, gives mass flow rate as a function of total pressure, total temperature, and critical area when the Mach number at the throat is know to be unity (Anderson, 1990:184).

$$\dot{m} = \frac{P_t A^*}{\sqrt{T_t}} \sqrt{\frac{\gamma}{R}\left(\frac{2}{\gamma+1}\right)^{\frac{\gamma+1}{\gamma-1}}} \tag{1}$$

By assuming that mass is conserved and with the knowledge that $\dot{m}=\rho AV$, equation 2 can be derived. This is very useful because it can be used to find the Mach number anywhere along the flow where the static properties are known.

$$M = \frac{\dot{m} RT}{pAa} \tag{2}$$

It is important to note that the acoustic velocity a for a perfect gas is equal to $\sqrt{\gamma RT}$. Another interesting property of isentropic flow (adiabatic and reversible flow) is the total temperature and pressure ratios, which are found in equations 3 and 4 respectively. With these relationships,

Mach number can be easily calculated if total pressure/temperature and local static pressure/temperature are known (Mattingly, 1996: 122).

$$\frac{T_t}{T} = \left(1 + \frac{\gamma - 1}{2} M^2\right) \tag{3}$$

$$\frac{P_t}{P} = \left(1 + \frac{\gamma - 1}{2} M^2\right)^{\frac{\gamma}{\gamma - 1}} \tag{4}$$

Oblique Shock Waves

Shock waves are the result of objects being placed in a supersonic flow. A common cause for the manifestation of this phenomenon is due to wedges being placed in supersonic flow. If the Mach number is high enough and the wedge is thin enough, the shock wave attaches to the wedge-shaped object to form an oblique shock wave. An illustration of an oblique shock wave can be found in figure 1 below.

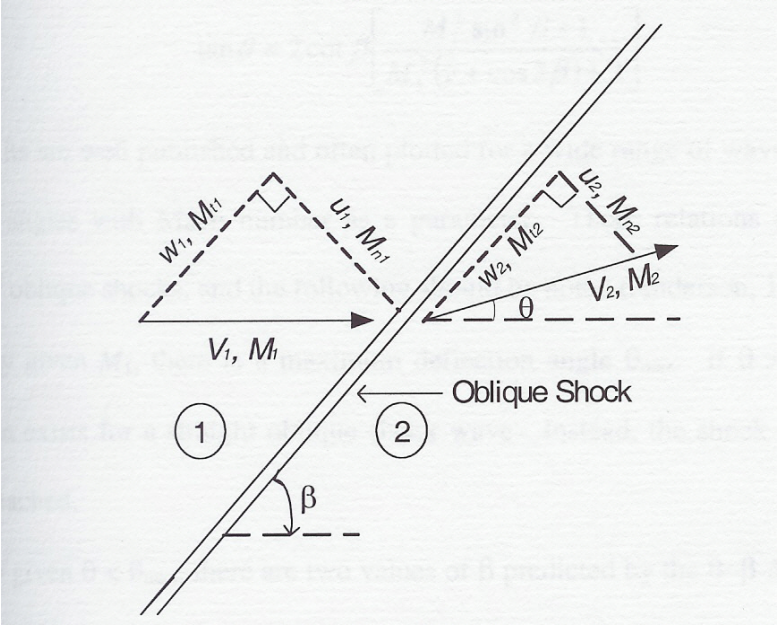

Figure 1 Geometry of an Oblique Shock Wave (Bautista, 2003: 2-2)

In this figure the upstream region is labeled 1 and downstream region is labeled 2. Ultimately the purpose of the oblique shock wave is to turn the incoming flow parallel to the wedge-half angle θ. In Figure 1 the velocity and corresponding Mach number in each region have been broken into components tangent and normal to the oblique shock wave and are denoted with subscripts t and n respectfully. Of note here is that the tangential component of velocity is preserved across the oblique shock wave (Anderson, 1990:105)

It has long been known that the downstream Mach number can be attained provided that the upstream Mach number and wedge half angle are known. The relationship between the upstream and downstream Mach numbers is known as the θ-β-M relations, seen in equations 5, 6, 7, and 8 below.

$$\tan\theta = 2\cot\beta\left[\frac{M_1^2\sin^2\beta - 1}{M_1^2(\gamma + \cos 2\beta) + 2}\right] \tag{5}$$

$$M_{n1} = M_1 \sin\beta \tag{6}$$

$$M_{n2}^2 = \left[\frac{M_{n1}^2 + \left(2/(\gamma - 1)\right)}{\left(2\gamma/(\gamma - 1)\right)M_{n1}^2 - 1}\right] \tag{7}$$

$$M_2 = \frac{M_{n2}}{\sin(\beta - \theta)} \tag{8}$$

Because these relationships are so vital to the evaluation of oblique shock waves, results for the θ-β-M relations have been published for a wide range of upstream Mach numbers and wedge-half angles (Anderson, 1990:106). Additionally, it is important to note the following (Bautista, 2003: 2-3,4):

1.) For a given M_1, there is physical geometry such that θ is larger than the maximum wedge-half angel θ_{max}. The result is a shock wave curved and detached in front of the wedge, in which case the oblique shock relations no longer apply.

2.) There are two values of β for any given θ that is less than θ_{max}. The larger of the two β values is known as the *strong solu*tion, while the smaller is called the *weak solution*. The solution that occurs is purely dependent on downstream pressure. It is this weak solution that is often favored in nature and therefore usually what occurs.

3.) If θ = 0, then β will either be 90^o (for a normal shock wave) or μ (for a Mach wave $\mu = \sin^{-1}\frac{1}{M}$).

4.) Lastly, for a fixed θ, there is a minimum Mach number where the flow is still attached; hence resulting in the largest wave angle (assuming a weak solution). If the free stream Mach number falls below this minimum Mach number, the flow will become unattached.

Reynolds Number

In aerodynamics there are myriad of nondimensional numbers that one could consider when trying to analyze a flow. One of the most important of these is the ratio of inertial to viscous forces, more commonly known as the Reynolds Number Re. The reason Reynolds number is so important is because it is used to determine if flow around two similar bodies are similar (Kuethe and Chow, 1998:364).

To derive Reynolds number, first consider a two dimensional incompressible flow with a boundary layer of thickness D. By starting with the full Navier-Stokes equations, the governing equation can be reduced to equations 9 and 10 below (Bautista, 2003: 2-7).

$$u\frac{\partial u}{\partial x} + v\frac{\partial u}{\partial y} + \frac{1}{\rho}\frac{dP}{dx} = \nu\left(\frac{\partial^2 v}{\partial x^2} + \frac{\partial^2 v}{\partial y^2}\right) \tag{9}$$

$$u\frac{\partial v}{\partial x}+v\frac{\partial v}{\partial y}+\frac{1}{\rho}\frac{dP}{dx}=\nu\left(\frac{\partial^2 v}{\partial x^2}+\frac{\partial^2 v}{\partial y^2}\right) \tag{10}$$

The inertial force terms, those on the left side of equations 9 and 10, $v\frac{\partial u}{\partial y}$, and so forth, have the dimensional form

$$\frac{\rho \mathrm{V}^2}{\delta}$$

where V is the velocity outside the boundary layer and δ is the characteristic length (usually the chord when flow is over an airfoil). The viscous force terms, those expressed by the group of terms on the right side of the equations, $\frac{\mu\partial^2 u}{\partial x^2}$, have the dimensional form

$$\frac{\mu \mathrm{V}}{\delta^2}$$

therefore the ratio of the two becomes the equation for Reynolds number, which follows in equation 11 (Kuethe and Chow, 1998:364).

$$\nu=\frac{\mu}{\rho}$$

$$\mathrm{Re}=\frac{\rho \mathrm{V}\delta}{\mu}=\frac{V\delta}{\nu} \tag{11}$$

Compressible Turbulent Jets

Compressible jets are the basis for achievement of high-speed flow. Development of that high-speed flow is quite complex. Figure 2 is an illustration of initial turbulent jet development.

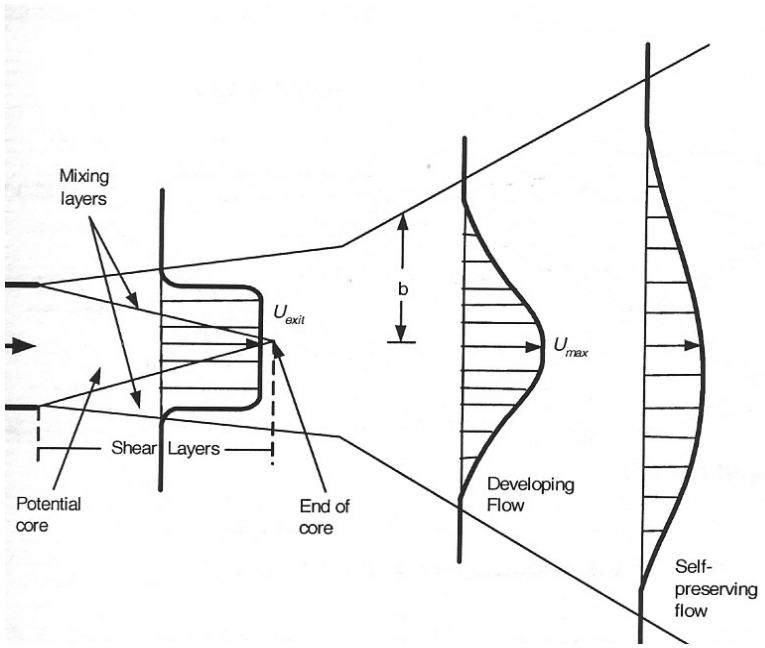

Figure 2 Initial Turbulent Jet Development (Bautista, 2003:2-8)

In Figure 2 velocity profiles are shown as the darker lines across the flow. As the jet issues a fully developed turbulent velocity U_{exit}, which is normally flat, a mixing or shear layer will form just at the edge of the nozzle exit. This shear layer will grow from the ambient fluid until it reaches the potential core flow with velocity U_{exit}. The shear layer will not grow for very long since the potential core dies out at about one nozzle diameter from the exit. At this distance, the potential core no longer has its distinctive flat shape, but rather transitions to the typical Gaussian-type shape. At approximately twenty diameters downstream of the exit, the velocity profile will reach a sustaining self-preserving shape (Bautista, 2003: 2-8).

With the knowledge of turbulent jet development, let us now focus on jet operating characteristics. Key to the performance of nozzles is the designed nozzle exit pressure P_{ne}. Ideally, one would like to operate a jet where P_{ne} would be the same as the receiver pressure/ambient pressure P_a. In this situation, there will be no pressure disturbances occurring

in the jet issuing form the nozzle; unfortunately, this rarely happens. Usually P_{ne} is lower or higher than P_a, in which case the following apply (Mattingly, 1996: 172).

1.) When $P_{ne} > P_a$ the jet is said to be *Underexpanded*. In this case a set of Prandlt-Meyer (PM) expansion waves develop at the nozzle exit, forcing the jet to expand; and thereby causing the jet to decrease in pressure. Following the PM expansion waves, oblique shock waves form starting at the jet boundary. This process repeats itself until self-preserving flow is attained.

2.) When $P_{ne} < P_a$ the jet is said to be *Overexpanded*. Here oblique shock waves will propagate from the nozzle exit forcing the jet to increase in pressure. Similar to the underexpanded case, a set of PM expansion waves will now emulate from the jet boundary. As before, this process will repeat itself until self-preserving flow is attained.

Below, in Figures 3 and 4, are illustrations of just such cases.

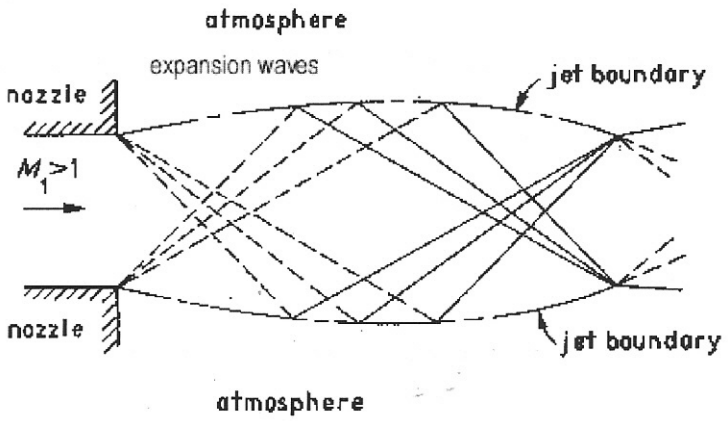

Figure 3 Underexpanded Jet (Bergren, 2002: 2-7)

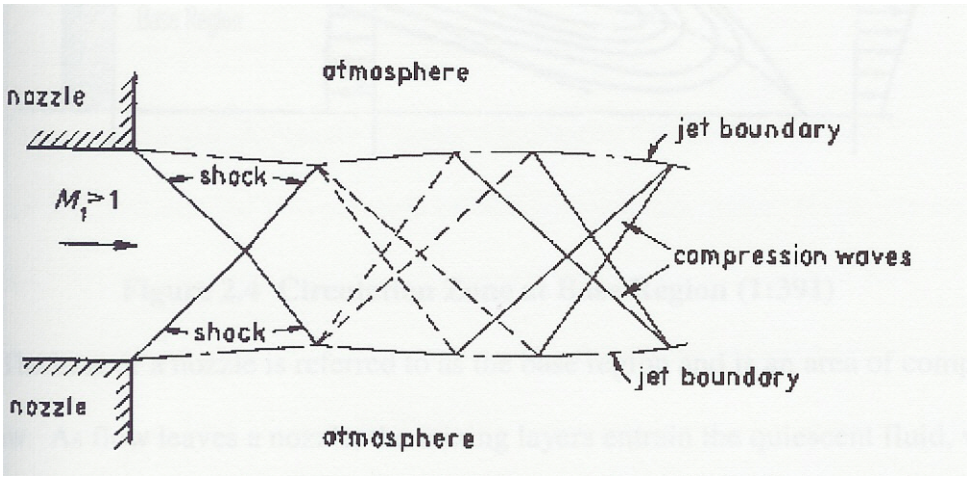

Figure 4 Overexpanded Jet (Bergren, 2002: 2-7)

Nozzle clusters or arrays are a collection of nozzles arranged in close proximity with one another. Because of their proximity these jets have a tendency to interact with each other creating "*a complex flow field of interacting shear layer, compression and expansion waves and turbulent mixing.*" (Bergren, 2002: 2-9) Moreover, since nozzles rarely operate at the on-design pressure, interaction between individual jets is an often occurrence. An example of a nozzle array operation at off-design conditions (overexpanded and underexpanded) can be found in Figure 5. From this figure, one can see that there is a flow void in the base region of the underexpanded nozzle array. The pressure in this region is below nozzle exit pressure, thus causing the jet to be underexpanded. If this pressure rises, it will cause the jets to separate as they will become overexpanded.

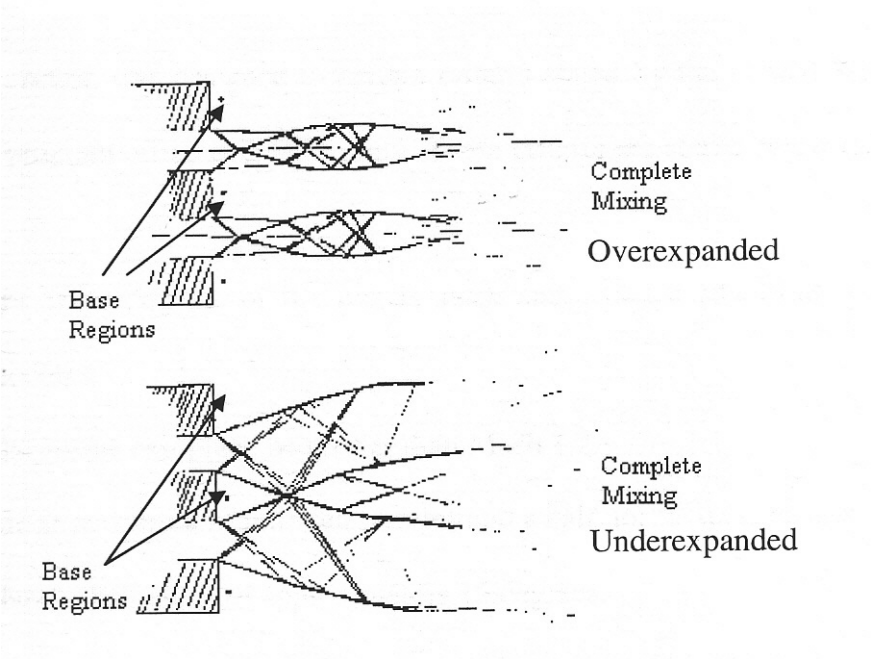

Figure 5 Nozzle Array

III. Procedural Methods

Test Section

The test section used here was a modified version of the test section that was specified by the United States Air Force SBL IFX program office and TRW, Inc. The original design criteria are listed below and are followed by modified design criteria (Bergren, 2002: 3-4).

1.) One quadrant or 90^o arc of the nozzle stack and Exhaust Manifold Assembly (EMA) be modeled.

2.) The flow at the nozzle exit plane be greater than Mach 1.2

3.) The nozzle array consist of ten nozzles; nine full nozzles and two half nozzles on each end.

4.) The nozzles have a half angle of approximately 15^o.

The modified design criteria are:

1.) The nozzle array will be flat and oriented parallel to the ground vice the original 90^o arc oriented perpendicular to the ground.

2.) Model previous nozzle geometry while incorporating as many individual nozzles as possible.

3.) Attach new nozzle array to existing Exhaust Manifold Assembly.

4.) The flow at the nozzle exit plane be greater than Mach 1.2

The new test section is shown below in Figure 6

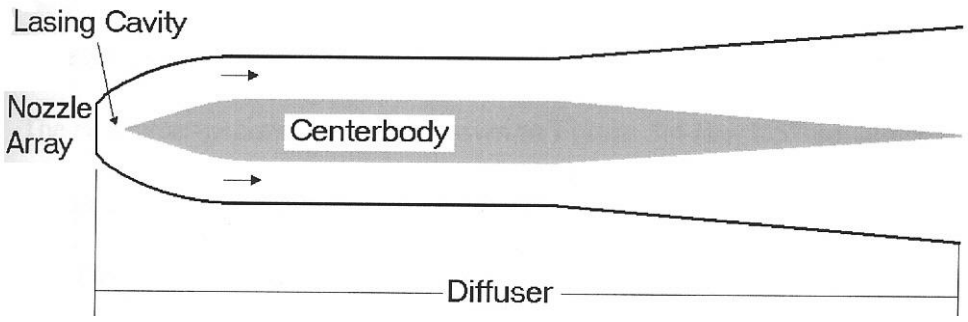

Figure 6 Cross-Sectional View of Modified Nozzle Array and EMA

Nozzle Array

Besides geometric similarities, the modified nozzle array shares some of the same operating conditions as the original scaled array. These conditions differ from the SBL IFX. As in the case of the $1/5^{th}$ scale nozzle array, the modified nozzle array does not have hydrogen injected into the exit flow during testing. Likewise air was used as the working fluid rather than fluorine molecules. Additionally, no lasing was to occur at the nozzle exit. The key objective in both cases was to produce similar Mach numbers at the exit plane (Bautista, 2003: 3-3). A cross-sectional view of the nozzle array can be found in Figure 7. Additionally Table 1 lists the critical dimensions for the nozzle.

Table 1 Nozzle Critical Dimensions (Bergren, 2003: 3-6)

	Description	Dimension
a	Base	4.6 mm
b	Exit Width	1.98 mm
c	Throat Width	1 mm
d	Half-Angle	15 deg

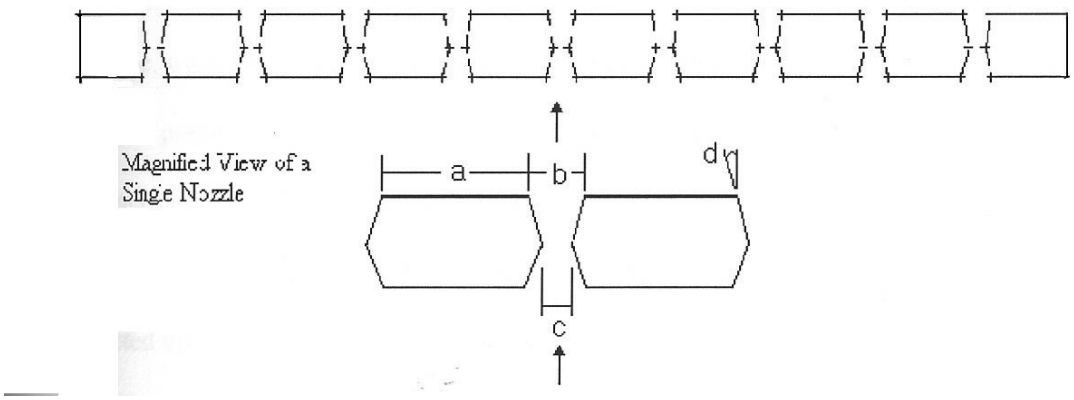

Figure 7 Nozzle Array Cross-Section (Bergren, 2002: 3-6)

This nozzle array arrangement works well to produce the higher Mach numbers; unfortunately, there are considerable losses with this setup. These losses, which can be attributed to viscous forces on the walls of the nozzle array, could have been abated if the nozzle walls were contoured (Bautista, 2003: 3-3). Regrettably, because the dimensions for this array were so small, fabricating contoured nozzles would be cost prohibitive. A preliminary study on this type of nozzle geometry was conducted by Captain Bergren, in which he determined a loss of approximately 15% due to non-isentropic flow. Figure 8 is a picture of the modified nozzle array in the vertical position. In this figure air is moving from the right to the left. Note that data collected with the nozzle in this position was used to compare with previous work. The focus of the experiment described in this report was written on data collected when this same nozzle array was rotated 90^{o}, so that the nozzles are parallel with the floor.

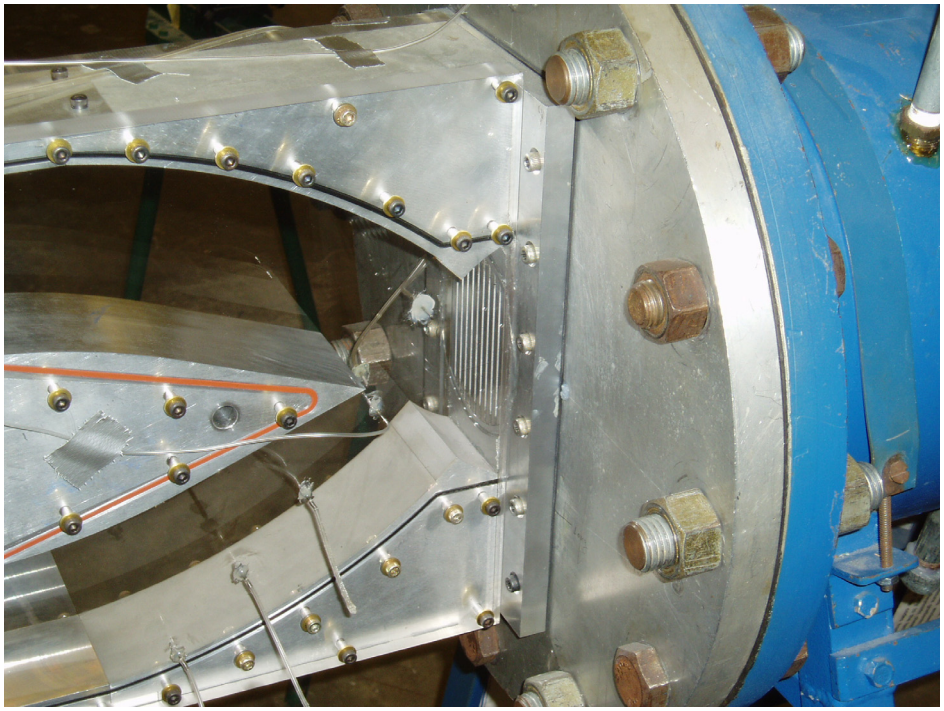

Figure 8 Experimental Nozzle Array

Downstream Components

The remainder of the downstream components consisted of the centerbody, the Exhaust Manifold Assembly (EMA), and a transition structure that was remodeled by Captain Bautista in 2003. The centerbody, which was used by both Captain Bergren in 2002 and Captain Bautista in 2003, was a symmetric airfoil designed to split the incoming flow into two channels, a top and a bottom. The leading edge was a wedge with a half angle of 21°. To ensure an airtight fit with the wind tunnel walls, gaskets secured by hex bolts were used. A sketch of the centerbody is below in Figure 9 to illustrate centerbody geometry.

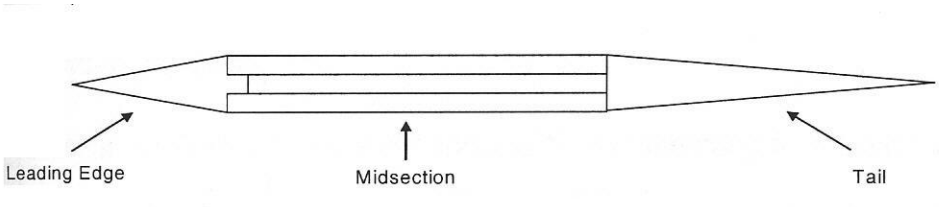

Figure 9 Centerbody (Bautista, 2003: 3-5)

The EMA, like the centerbody, was used in previous studies conducted by Captains Bergren and Bautista. The EMA houses both the nozzle array and the centerbody. Initially, the viewing area extended only 30.5 cm downstream of the nozzle exit. It was modified by Captain Bautista by replacing the first 76 cm of the walls with optical grade Plexiglas™ for improved viewing. TRW Inc. designed and provided the contour for the top and bottom of the diffuser. These parts were designed to redirect the radial flow from the original 1/5th scale model nozzle array while minimizing losses (Bautista, 2003: 3-6). Although the same diffuser was used, the top and bottom contours can be changed to investigate future designs for redirecting flow. In total, the EMA was 1.41 meters long and ranged in height from 33.3 cm at the nozzle exit plane to 47 cm at the transition structure. A picture of the EMA is shown in Figure 10.

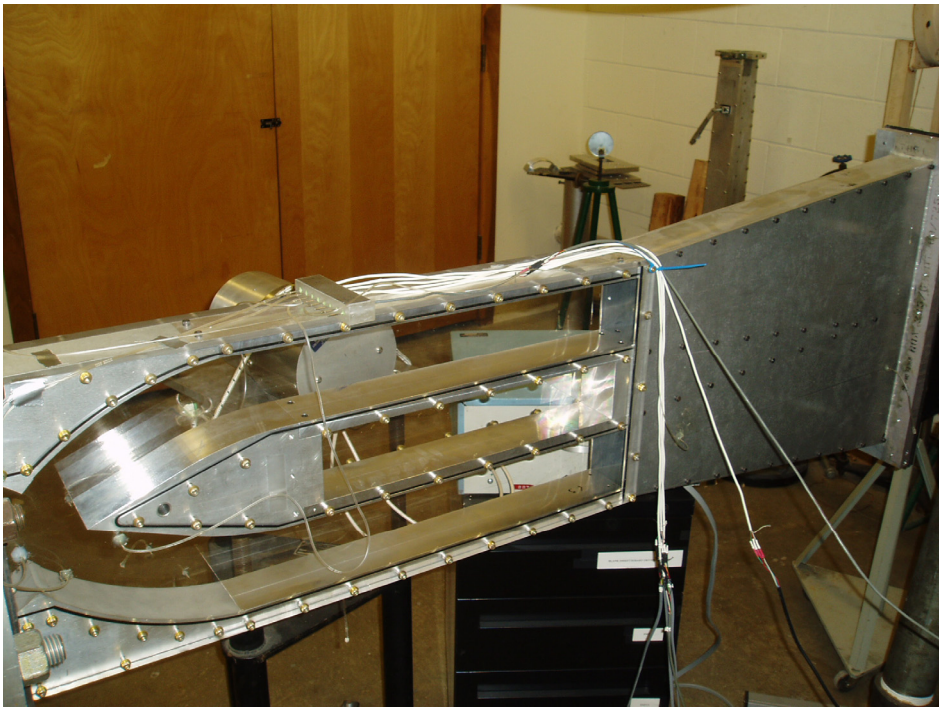

Figure 10 Exhaust Manifold Assembly

The last section of the downstream components was the transition structure. For this study the remodeled transition structure, designed by Captain Bautista, was used. Since it had a

large enough exit area to enable sustained supersonic flow at the nozzle exit for a longer period of time. The original transition structure had a 108.6 cm^2 rectangular exit area, while remodeled transition structure has a 285 cm^2 circular exit which was identical to vacuum line entrance, thus allowing for only one choke point, the nozzle throat. A photograph of the transition structure and vacuum line entrance are found below.

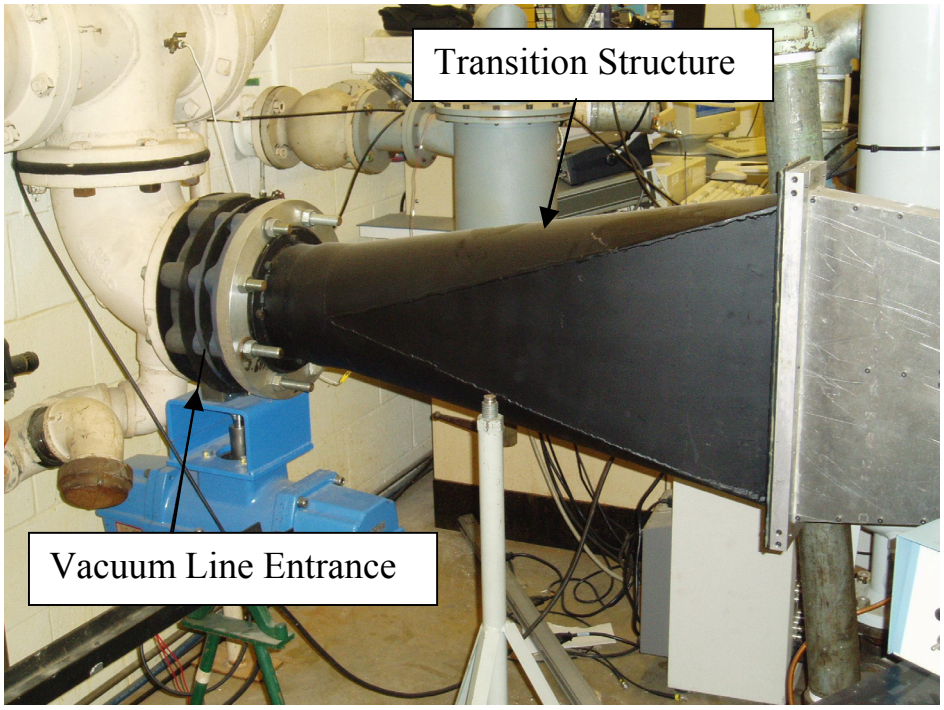

Figure 11 Transition Structure and Vacuum Line

Wind Tunnel System

The wind tunnel used in this study was comprised of three major subsystems: a compressed air system, a pressure regulation system, and a vacuum system. A schematic of the wind tunnel is shown in Figure 12. In addition to this schematic, Table 2 lists the manufacturer and model number for the components of the subsystems used in this wind tunnel. This particular system is a blow-down/vacuum system, and when used in conjunction with the nozzle

array described previously, could produce a maximum steady state mass flow rate of approximately 0.25 kg/s.

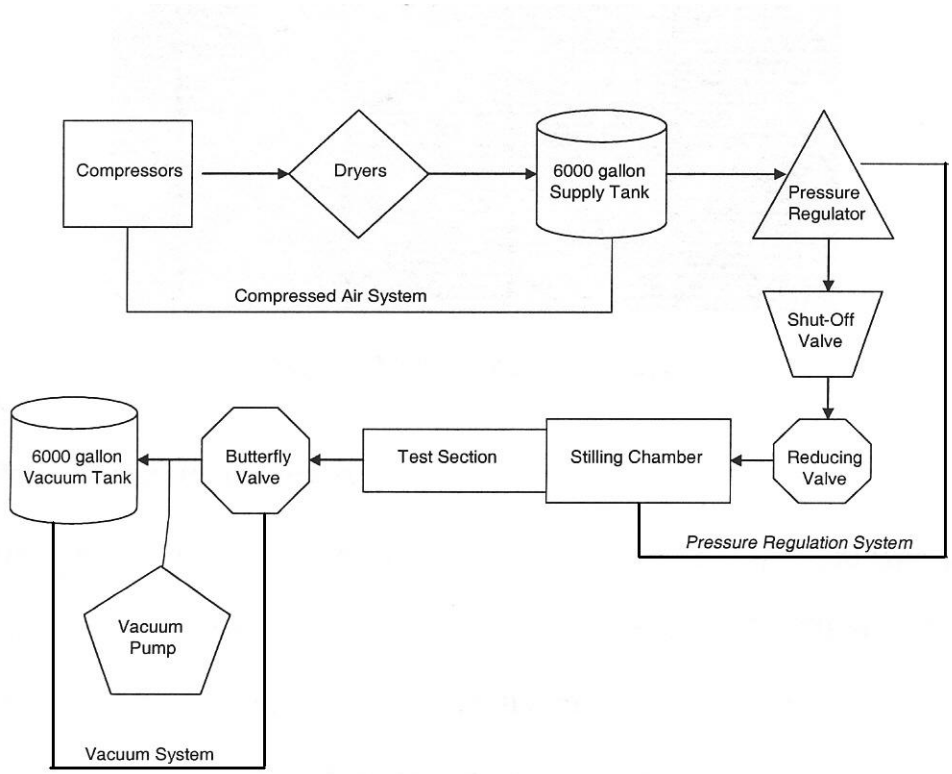

Figure 12 Wind Tunnel Schematic (Bautista, 2003: 3-9)

Table 2 Wind Tunnel Components

Item	Manufacturer/Description	Model number (If available)
Air Compressor	Ingersoll-Rand	SSR HXP 50 SE
Air Dryers	Ingersoll-Rand	N/A
Compressed Air Tank	6000 Gallon compressed air tank	N/A
Pressure Regulator	diaphragm-type pressure regulator	N/A
Pressure reducing valve	2 in air loaded pressure reducing valve	N/A
Stilling Chamber	12 in Stilling Chamber	N/A
Shut-off Valve	Manual shut-off valve	N/A
Vacuum Tank	6000 Gallon vacuum tank	N/A
Vacuum Pump	Stokes two stage pumping unit	412-11
Butterfly Valve	Pneumatically operated butterfly valve	N/A

The compressed air subsystem starts with the Ingersoll-Rand compressors. Set to an output pressure of 140 psi, these compressors feed the high-pressure air into the air dryers. Here, compressed air is dried and filtered to prevent particle and moisture damage to the rest of the system. The dried and filtered air is then passed through to the compressed air tank where it is stored at the compressor output pressure until the control valve is opened.

The pressure regulation subsystem is used to control the flow of air and to reduce tank pressure to a usable level. This is accomplished through the means of a diaphragm-type pressure regulator that reduces air pressure to 90 psi. To reduce the inflowing air pressure to a usable level, a 2 inch, air loaded, pressure-reducing valve was used. This valve is operator controlled via a digital gauge. With the valve, the operator could accurately set the stilling chamber pressure. The stilling chamber, in conjunction with a flow straightener, provided conditioned air to the test section. A shut-off valve was used to start and stop the flow into the test section.

To provide a vacuum for the wind tunnel, a Stokes two-stage vacuum pump was used to evacuate the vacuum tank. This subsystem supplies the wind tunnel with a 6000 gallon vacuum at a pressure of 0.03 psi. When the butterfly valve was opened and compressed air was flowing, the wind tunnel could run for roughly 45 seconds before the vacuum tank would fill up and the Mach number at the nozzle exit would fall below the minimum Mach number desired for this experiment.

Data Collection

Two types of data were collected in this study; one type was schlieren images of the viewing area. The second type was static pressure measured at various points along the walls of the wind tunnel with pressure transducers (PTs). The pressure transducers were positioned in places where pressure data could easily be correlated with the schlieren images. Because of the

high-speed nature of the fluid in this study, rapid data acquisition was a necessity. A list of test equipment used is given in Table 3.

Table 3 Test Equipment

Item	Quantity	Manufacturer	Description	Model Number (If available)
Pressure Transducers (PT)	3	Endevco	piezoresistive PT's for absolute pressure	8530C - 15
Pressure Transducers (PT)	2	Endevco	piezoresistive PT's for absolute pressure	8530C - 50
Pressure Transducers (PT)	1	Endevco	piezoresistive PT's for absolute pressure	8350Z -100
Signal Conditioner	6	Endevco	signal conditioner for Endevco PTs	4428A
Data Acquisition System (DAS)	1	Nicolet	mulit-channel data acquisition software and A/D board	Nicolet MultiPro 120
Personal Computer (PC)	1	Gateway 2000	386 pc running windows 3.1	N/A
Schlieren Lamp	1	Aerolab	cylindrical filament schlieren lamp	N/A
Mirror	2	N/A	80 in focal length high quality mirror	N/A
Knife Edge	1	N/A	vertical knife edge	N/A
Digital Camera	1	Photron	Photron FASTCAM-X digital camera	1280PCI
Personal Computer (PC)	1	Dell	Pentium III pc running Windows XP	N/A
Digital Image Capturer	1	Photron	PFV Photron FASTCAM viewer software	N/A

Pressure Data

Figure 13 depicts the location of five pressure transducers used in this experiment. A sixth transducer, not shown in Figure 13, was located in the settling chamber.

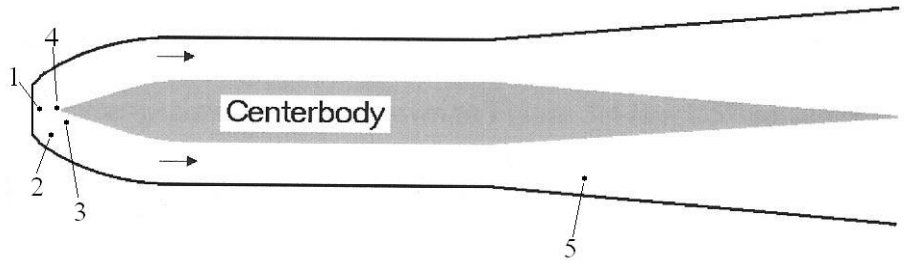

Figure 13 Pressure Transducer Location

Using the Nicolet computer program and the pressure transducers, pressure data were collected at a sampling rate of 1 kHz for fifteen seconds thus yield 15000 points of time stamped pressure readings. A fifteen second sampling time was chosen based on initial runs with the new nozzle array; which showed that the flow remained attached for approximately eleven seconds. A fifteen second sampling time would be able to capture the entire run while the flow was attached. These particular pressure transducers recorded absolute pressure; however, PTs 1, 2, and 3 had a range of 0-15psi. PT 4 and 5 had a range of 0-50 psi and PT 6 (settling chamber) had a range of 0-100 psi. The reason various ranged pressure transducers were used is because they were the only available pressure transducers that all read absolute pressure.

The Nicolet Data Acquisition System (DAS) was capable of collecting 16 simultaneous data channels on 4 separate MP 120 channel cards. Each card had 4 channels labeled A, B, C, and D. The pressure transducers were arranged as such: PT1 channel 1A, PT2 channel 1B, PT3 channel 1C, PT 4 channel 3A, PT5 channel 3B, Stilling Chamber channel 3C. Channel two was skipped because the board was bad. Overall the data signals were evenly divided between channels 1 and 3 to minimize the workload of each channel. Each PT signal was conditioned and amplified by the Endevco signal conditioners, after which the DAS would digitize the data, which could then be stored on digital media.

Schlieren Data

Due to the high density gradients associated with supersonic flow and resulting shock activity, pictures of the shock structure were taken using the schlieren photographic technique. A diagram of the particular schlieren setup used in this study can be found below in figure 14.

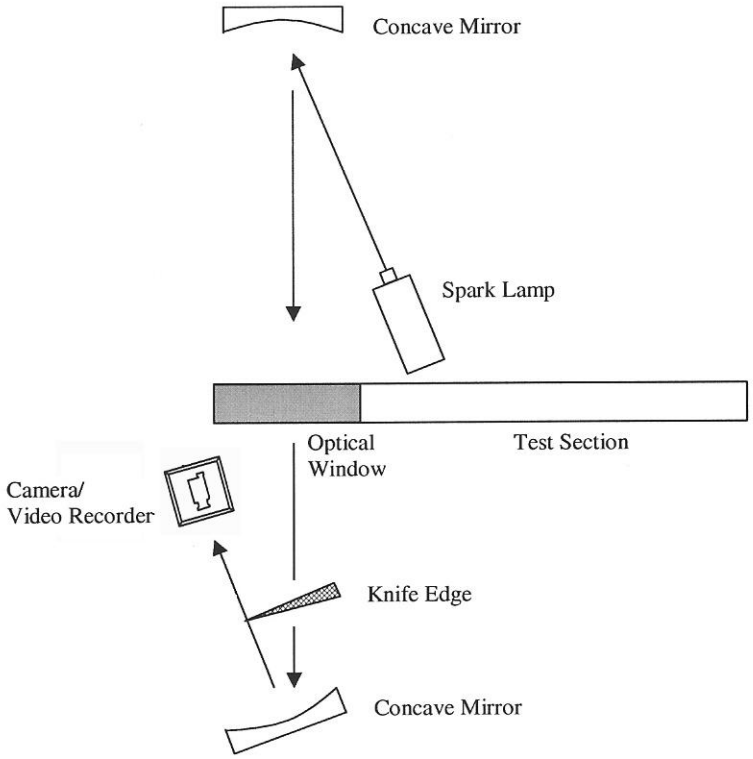

Figure 14 Schlieren Photography Setup (Bergren, 2002: 3-11)

The lamp for this study was oriented such that the cylindrical filament was vertical. Although an ideal light source would be a point source for best quality pictures, the cylindrical filament did yield images that were quite good (Bautista, 2003: 3-14). To acquire these high quality pictures the knife edge needed to be oriented the same as the filament, hence the knife edge was placed in the vertical position. Possibly due to light source orientation, the best images were produced when the knife edge cut the right half of the image rather than the left. The angle between the light source and the mirrors are critical to image clarity. By keeping the angle between the light

source and the mirrors small, image distortion was kept to a minimum. These conditions were also used in the two previous studies conducted by Captains Bergren and Bautista; however, three significant changes were made from those studies to this. The first was that the images were directly captured from the light source, as opposed to being captured from a viewing screen. This increased the light intensity of the images. Secondly, the digital camera software frame rate used in this study was increased significantly from 60 frames per second in the two previous studies to 1000 frames per second. Lastly, the shutter speed was increased in the digital camera software from 1 Hz to 128 kHz. These three improvements gave a vast improvement in image quality and resolution. Like before, still shots were taken from the digital video stream and will be showcased later.

Experimental Procedure

The second objective of this study was accomplished via one set of procedures repeated eight separate times. During each of the eight runs, a pressure transducer was position on the stilling chamber to measure stagnation/total pressure in the system.

Calibration and Uncertainty

Prior to testing, all six pressure transducers were calibrated using a portable pneumatic pressure tester. Each transducer was tested at two different pressure levels, one above and one below atmospheric pressure. Because testing only took two days, the transducers needed calibration only once. Capt Bergren performed a detailed uncertainty analysis of pressure readings during his research, it is included in this report and found in Appendix A. The uncertainty associated with bias in the pressure transducer and precision error in the signal conditioner was mitigated to ± 0.3 psia. Because pressure was used to calculate mass flow rate

and Mach number, the error associated with the pressure readings will propagate into those calculations.

Wind Tunnel Operation

There were three main categories of wind tunnel operation that were followed for this study. Two involved instrumentation while the third was the actual operation of the wind tunnel itself. It is important here to note that prior to each run, the vacuum system and the compressed air system were turned on and allowed to reach a steady state. Additionally, all valves in the system were initially closed.

Before any runs, the DAS and schlieren systems were adjusted to the appropriate settings. These settings can be found in Table 4.

Table 4 Initial Instrument Settings

Nicolet DAS		
	Procedure No.	Procedures
	1	Open Nicolet (Nic Win)
	2	File - open channel Setups - dave1.chs
	3	File - open display setups - dave1.dss
	4	check for channels 1 (A-C) and 3 (A-C)
Schlieren System	Procedure No.	Procedures
	1	Turn on schlieren Lamp (Be sure to wear UV protection glasses)
	2	Open Mirror covers
	3	Check to make sure light beam completely covers the test section
	4	Open PFV software
	5	Check live as camera source
	6	Set frame rate to 1000fps
	7	Set shutter speed to 1/128000 sec
	8	Using a warm object like hot water, check quality of schlieren image

Once the initial setup was complete, the tests could then begin. Operations done out of order could possibly destroy the Plexiglas™ walls of the test section; therefore, it was critical that the procedures were followed exactly.

First, the vacuum butterfly valve is opened and the tunnel subjected to a vacuum. Second, the shut-off valve is opened to allow compressed air to flow. Next, use the live images from the digital camera to verify that air is flowing and is supersonic. Verify supersonic airflow, check the OneShot button on the DAS system and choose OK. Acquire pressure data by pressing Ctrl-T. Once that pressure data collection has started, collect schlieren images by choosing the save option on the PFV software. After fifteen seconds the DAS system would stop collecting data automatically at which time the schlieren data collection can be stopped. Next, shut off the compressed air system by closing the appropriate valve. Lastly, wait approximately two to three seconds then shut off the vacuum system valve. As a side note, it is very helpful to have a second person run the schlieren system so that the maximum amount of usable data could be taken before the vacuum tanks fill up. This process was repeated for pressure-reducing valve settings (PRVS) from 30 psia to 15 psia in increments 5 psia. Each pressure-reducing valve setting was tested when the flow was attached and unattached to the centerbody. Pressures denoting the attached cases will have a subscript a, those denoting unattached cases will have a subscript u.

Data Conversion

Because the DAS is such an old system, the data it collects must be converted into a form readable by other computers and programs. Data is converted taking the saved pressure data and passing it through the WaveCon program. This program will convert the pressure data to a tab delimited form that can then be read by programs like MatLab or Microsoft Excel. Once converted the data can be processed.

IV. Results

Pressure Data

The one adjustable variable that has the largest effect on nozzle exit Mach number is the stilling chamber pressure. This is because exit Mach number is directly proportional to mass flow rate, which in turn is directly proportional to total pressure (stilling chamber pressure). Below in Figure 15 is a time-based graph of typical total pressure, which was taken for a pressure-reducing valve setting of 30 psia. Although, the valve setting for this graph was 30 psia, all other runs were similar in shape to the one pictured here.

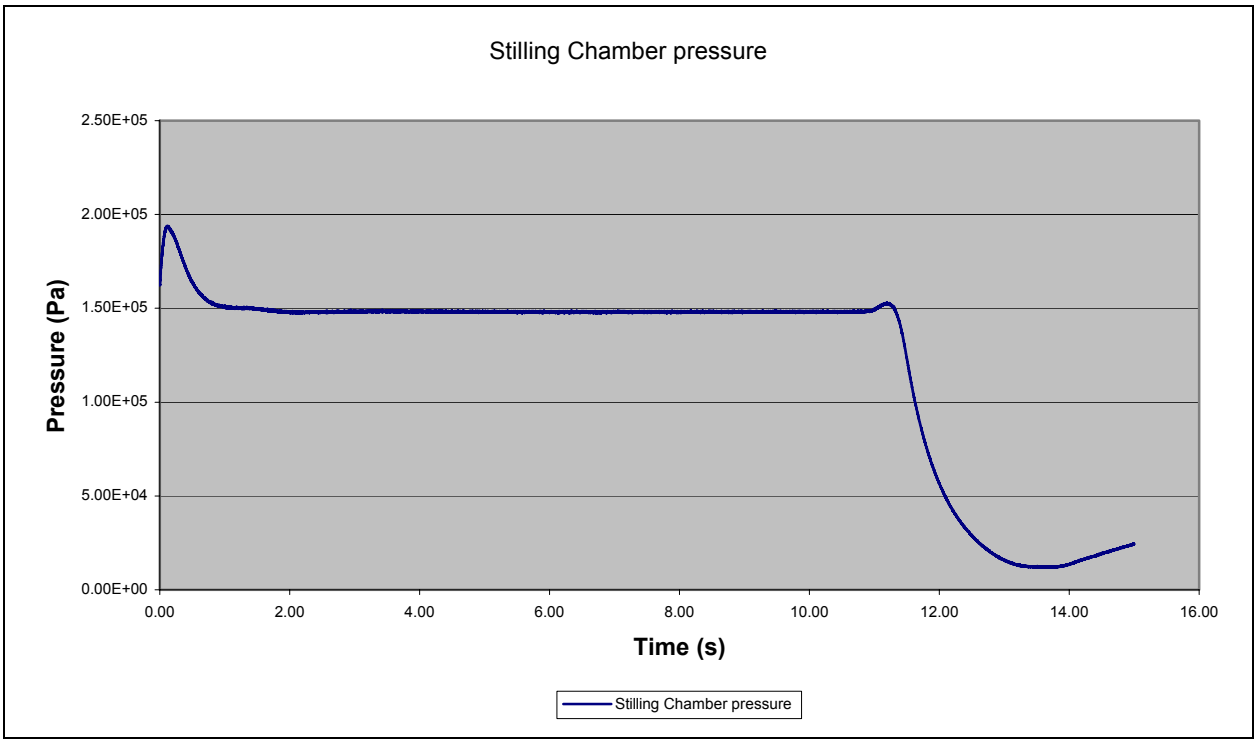

Figure 15 Typical Stilling Chamber Pressure

In the first seconds of any given run, as in this one, there were some transient pressure readings. These were due to the mechanical feedback loop of the pressure reducing valve and usually died out by two seconds (Bergren, 2002: 4-2). After the initial transient readings the pressure would

reach a steady state. As stated before, there is a ± 0.3 psia (2kPa) uncertainty with these readings. Please note that the Mach number was assumed to be unity at the throat for all runs.

From equation 1 it can be seen that mass flow rate is directly proportional to total pressure. Therefore the same sort of transient followed by steady state behavior is expected. Figure 16 is a typical mass flow rate graph. The values used to create this graph were those for values at the throat and the same pressure-reducing valve setting as for Figure 15.

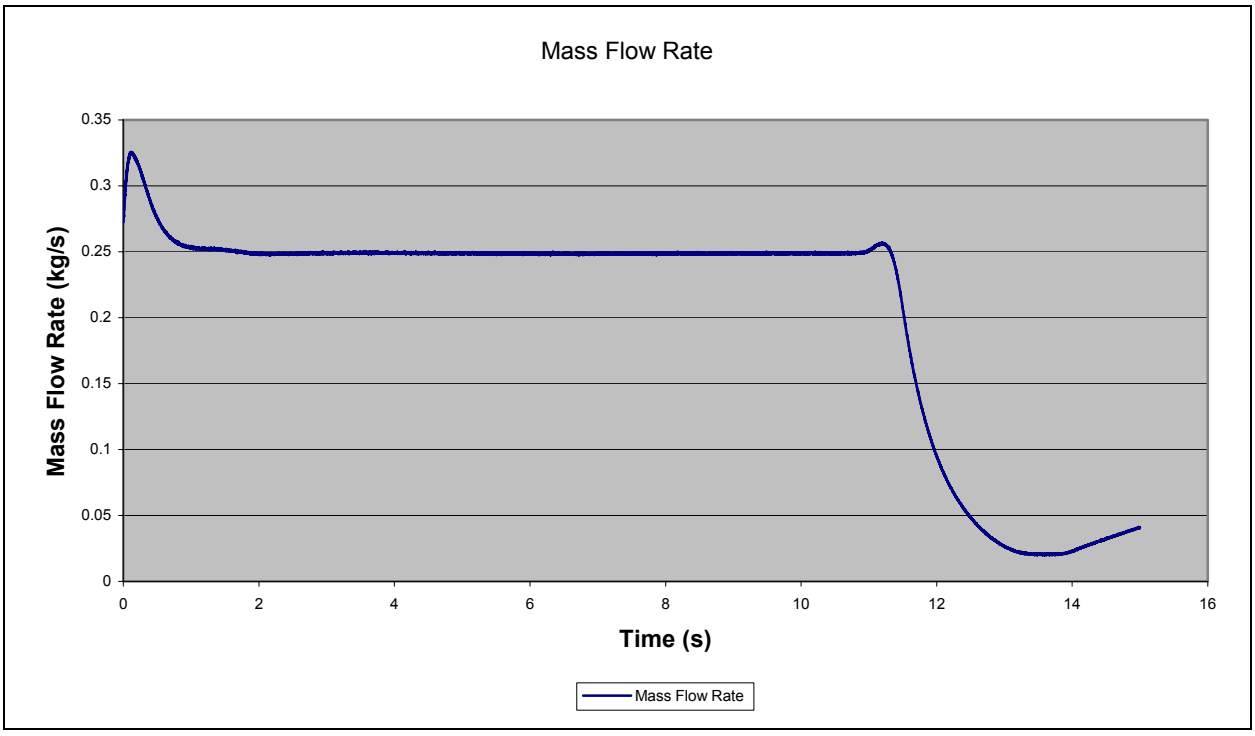

Figure 16 Typical Mass Flow Rate

The temperature used to calculate the mass flow rate for these experiments was the outdoor ambient air temperature (approximately 271 K). Capt Bergren determined the maximum error for the mass flow rate calculations to be ± 4.7 g/s. These calculations are listed in this report in Appendix A. One may notice that around 11 seconds into the run the pressure and mass flow exhibit a sharp jump followed by a steady decrease. This sharp jump is the point in time where

the flow becomes unattached. Consequently, the tunnel is shut down causing the steady decrease.

Pressure readings from the pressure transducers were used to determine a local Mach number at the various locations along the wind tunnel. Because of the various flow regimes throughout the wind tunnel, the Mach number at each transducer location was calculated with different equations. Equation 4 was used to calculate the Mach number at transducers locations 1 and 4 because they were in the core flow. These values were reduced by twenty percent for non-isentropic flow losses, which were discussed in chapter 3. Equations 5 through 8 were used to calculate the Mach number a location 3 because it was just behind an oblique shock wave. Lastly, the Mach number at location 5 was calculated with equation 2. The local cross-sectional area at location 5 was 0.015 m^2. These Mach numbers could then be graphed as functions of time. Figure 17 is a graph of local Mach number as a function of time; where, the location of each transducer has been identified in Figure 13. The Mach number for transducer 2 was not graphed. This is because transducer 2 was located in the shear layer of the jet and no suitable method was found to calculate the Mach number in this region.

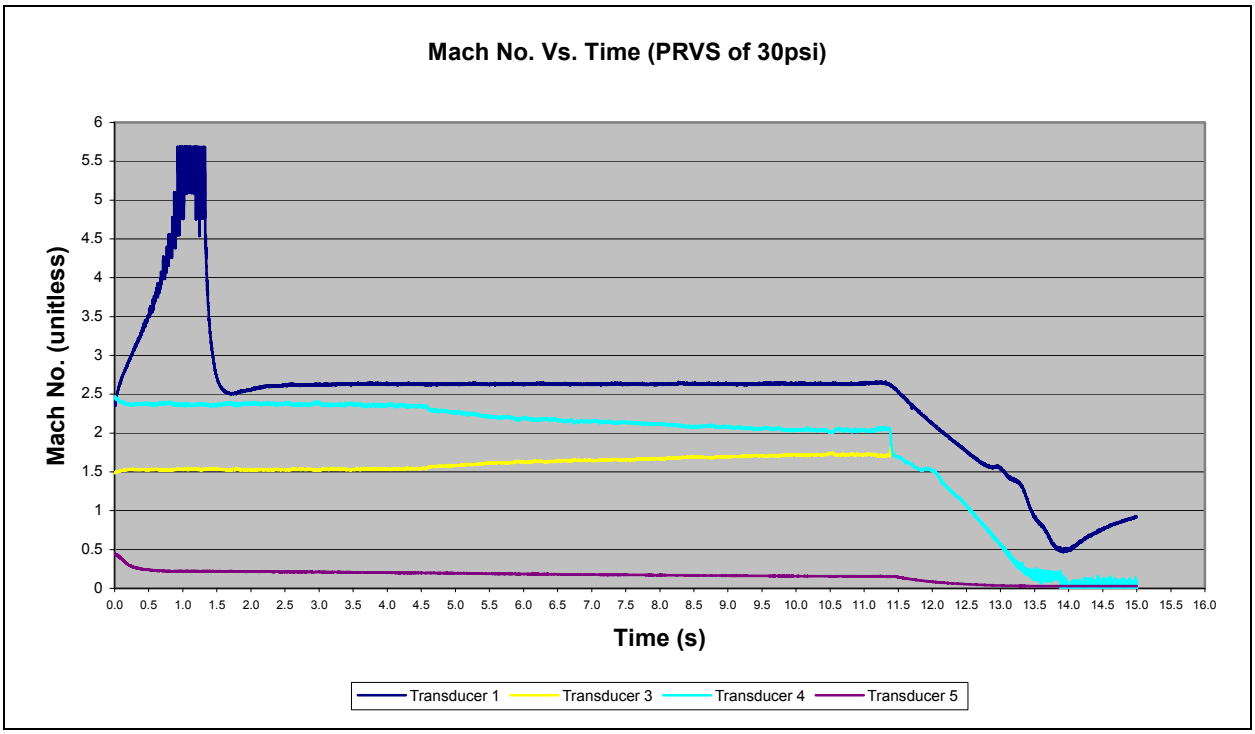

Figure 17 Local Mach Number

It can be seen from this figure that the Mach number at location 1 was highest. This was expected since that location was immediately downstream of the nozzle array exit. The initial spike in Mach number here can be attributed to the mechanical feed back of the pressure-reducing valve, much in the same way that stilling chamber pressure or mass flow rate spike at the beginning of a run. The reason this phenomenon is not seen in any other transducer location is because of their proximity to the nozzle exit. Transducer 1 is right at the nozzle array exit, whereas all others are farther downstream. After this initial spike, the Mach number reaches a steady state of approximately 2.65 until the compressed-air system is shut off. Mach numbers at locations 3 and 4 are also what would be expected. Mach numbers at location 4 are lower than at location 1 because by the time the compressed air has moved to location 4 some of its energy has been dissipated to the surrounding fluid. Mach numbers at location 3 are lower than those at 4 because they are behind the oblique shock wave that forms on the leading edge of the

centerbody. Lastly, Mach numbers at location 5 are well below the sonic condition because the cross-sectional area at location 5 is over two orders of magnitude larger than the nozzle throat area.

Schlieren Images

A schlieren optical system was used to capture images and video of the flow field in the optical cavity during wind tunnel operation. Initially digital video of the flow field was captured, after which the Photron FASTCAM Viewer (PFV) software allowed the user to pull off individual still images from the video.

Vertical and Horizontal Nozzle Array

In previous studies faint radial lines were seen just aft of the nozzle array. It was suspected by Captain Bergren that these were intersecting shock waves and expansion fans, Captain Bautista on the other hand hypothesized that they were simply radial expansion waves (Bergren, 2002: 4-11 and Bautista, 2003: 4-21). Neither of which could be proven or disproven due to the fact that schlieren images could not be taken in the correct place to see the nozzle interactions. Because the nozzle array designed for this study could be rotated about a vector normal to the nozzle array exit plane, this could be investigated. This nozzle array, while in the vertical position, resembles what would be seen from the $1/5^{th}$ scale model. In the horizontal position, interactions between the nozzles can be seen. Nozzles in the horizontal position do not resemble any previous configuration. This configuration was purely used for observations. As is turns out, Captain Bergren's suspicion was correct. The Figures 26 and 27 show the nozzle array used in this study in two configurations. In Figure 26, where the nozzles are aligned vertically, the same faint lines that were observed in previous studies are seen here. Figure 27 shows the complex flow field of the nozzle array in the horizontal position. The intersections of shock and

expansion waves can be seen at roughly the same intervals as the faint lines. Leading to the conclusion the faint lines are the result of intersecting shock and expansion waves.

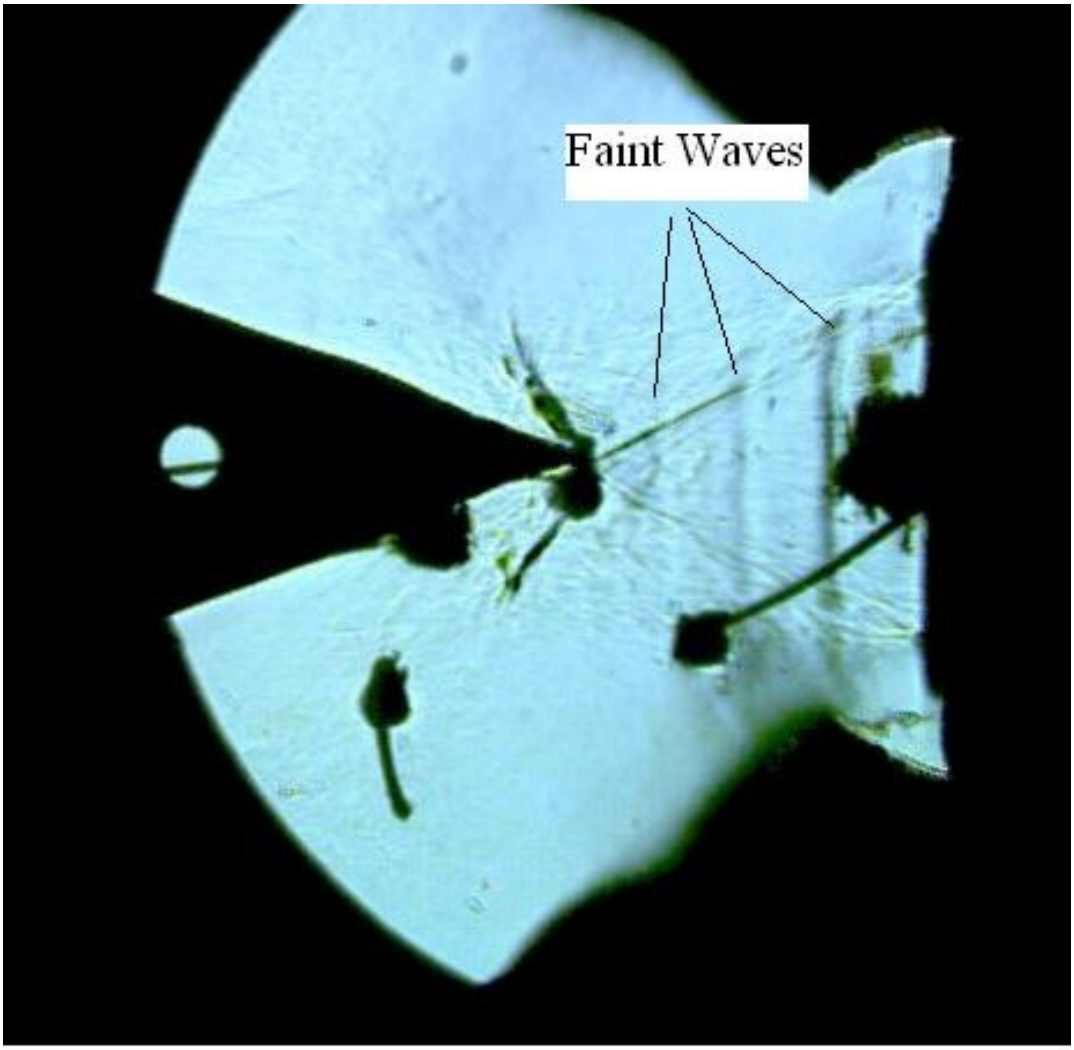

Figure 18 Nozzle Array in Vertical Position

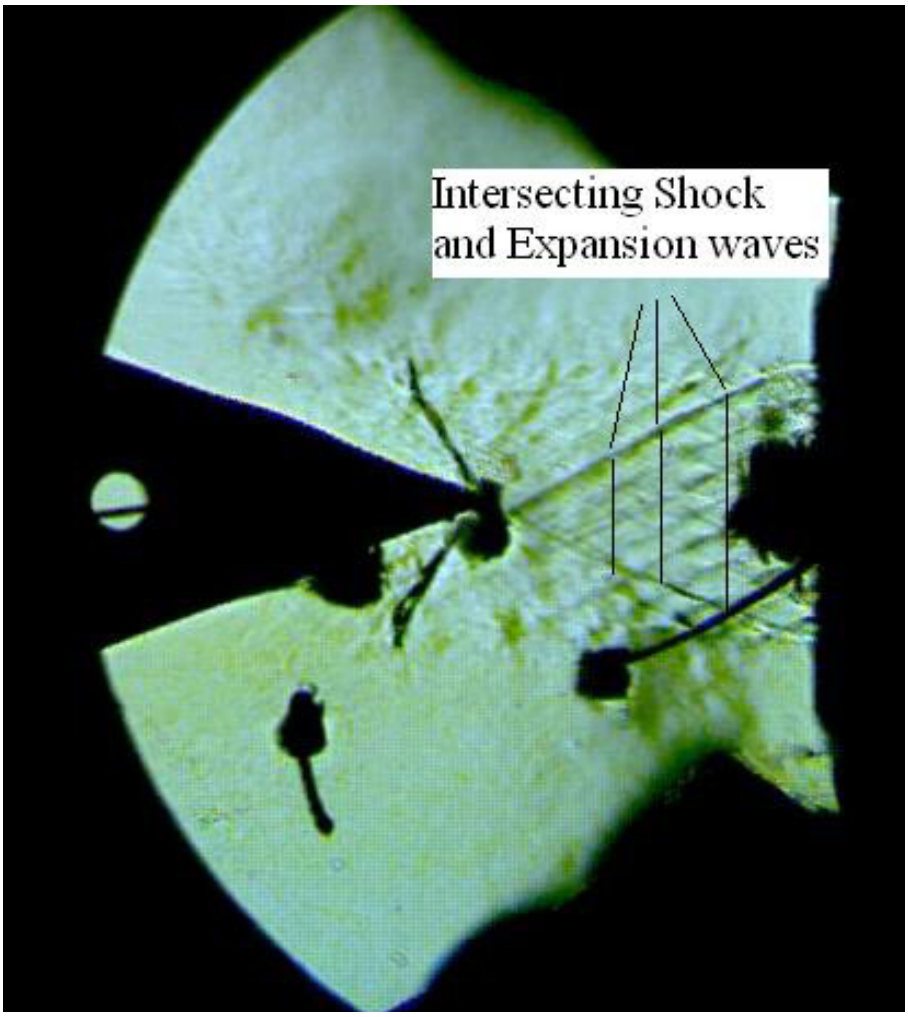

Figure 19 Nozzle Array in Horizontal Position

Oblique Shock Waves

The oblique shock wave attached to the leading edge of the centerbody could be used to verify Mach number calculations. Figures 18 through 21 are images captured for four different pressure-reducing valve settings; 30a, 25a, 20a, and 15a psia respectively. In each of these cases the flow is attached to the centerbody.

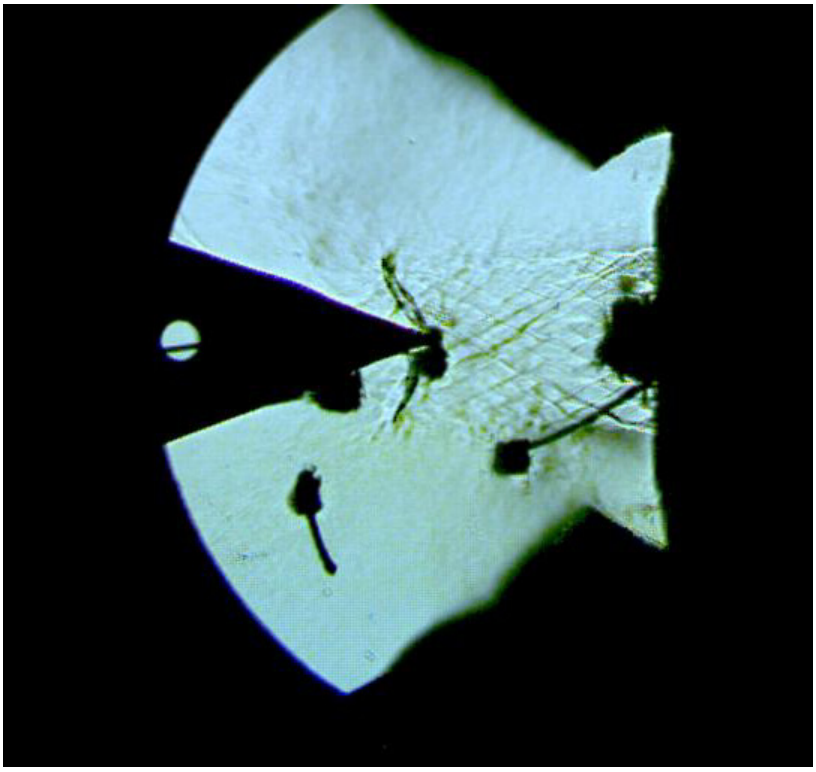

Figure 20 Schlieren Photograph for PRVS of 30a (M_4 = 2.18)

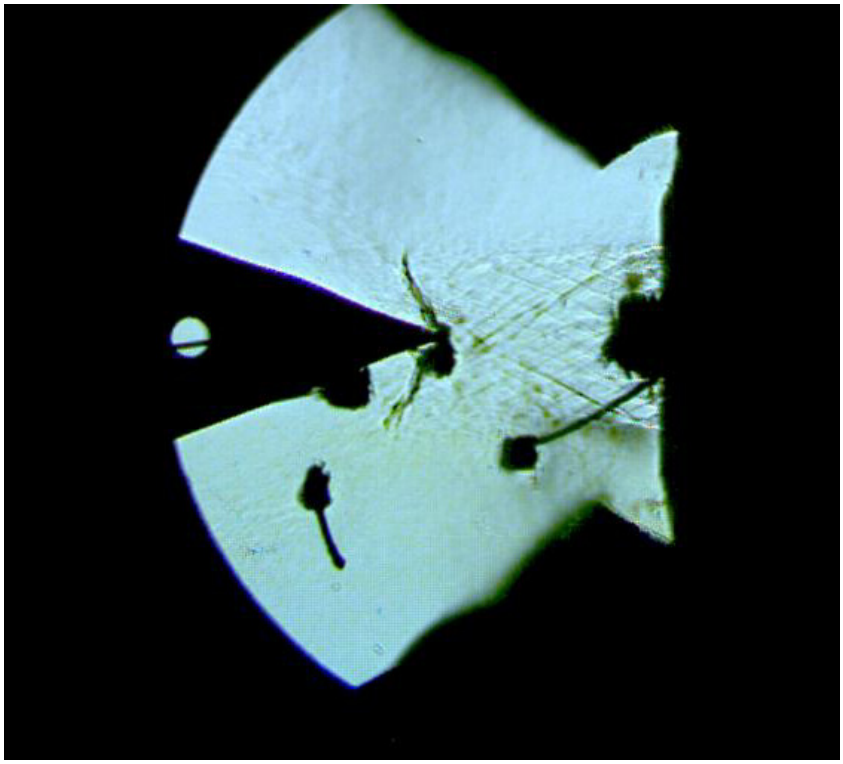

Figure 21 Schlieren Photograph for PRVS of 25a (M_4 = 2.11)

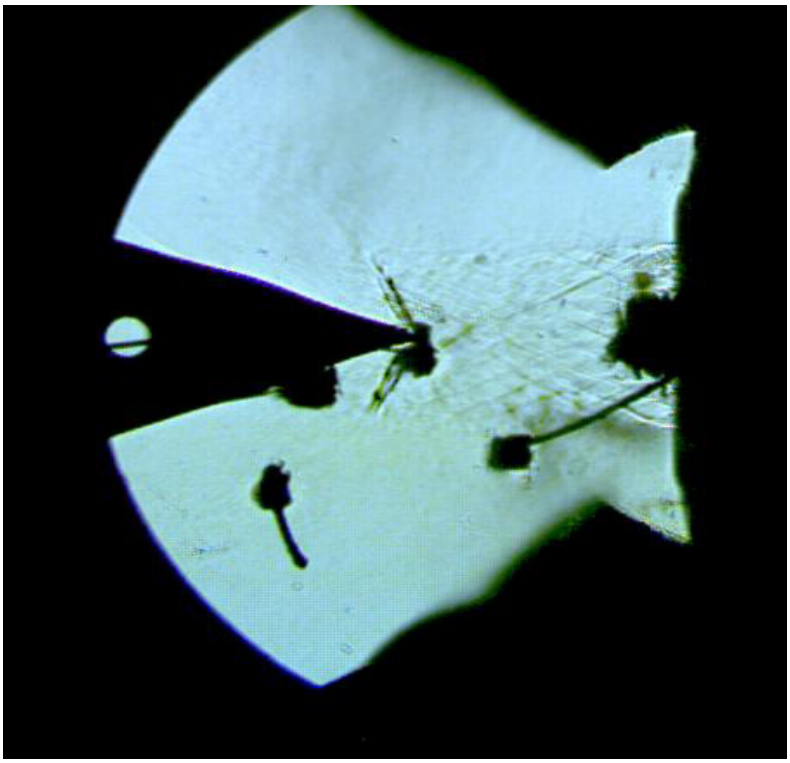

Figure 22 Schlieren Photograph for PRVS of 20a (M_4 = 1.97)

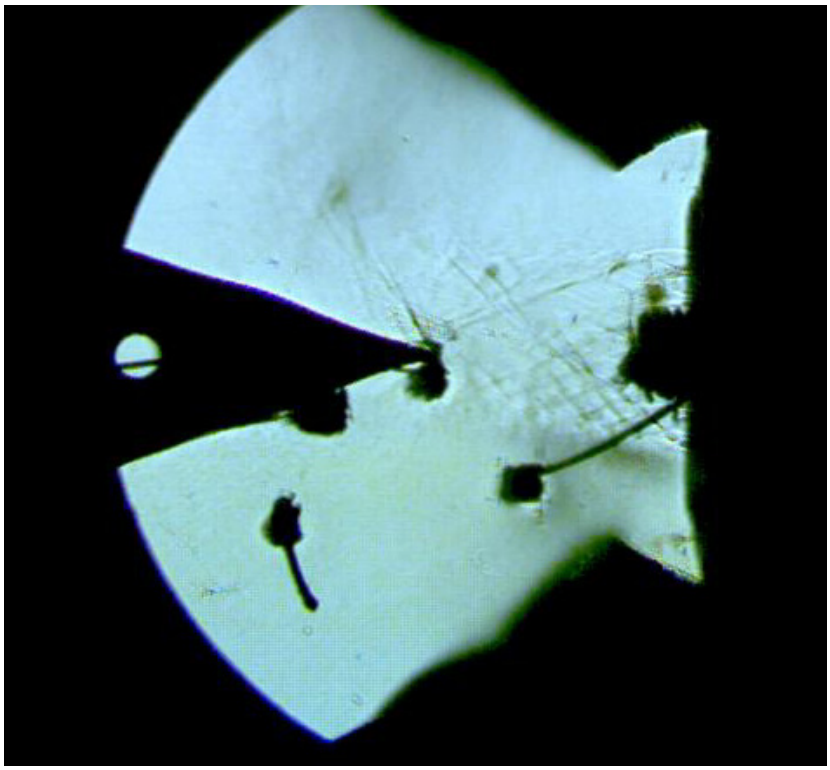

Figure 23 Schlieren Photograph for PRVS of 15a (M_4 = 1.91)

These images, taken while flow is at a steady state, illustrate the subsiding of the shock diamond as the pressure-reducing valve setting was reduced. Moreover, they also illustrate the intricate interactions of the individual nozzles within the array. A third important fact that can be deduced from these photographs is the fluid Mach number at the leading edge of the centerbody. By measuring the wave angle and the wedge-half angle an iterative process can be used to determine the Mach number of that flow. Additionally, the Mach numbers determined via these images correspond well with those calculated using pressure data. This fact further justifies Mach numbers calculated via the use of pressure measurements.

Unattached Flow

Eventually, the vacuum tanks will fill up to the point where the vacuum pumps can only evacuate the incoming air. At this point a large pressure ratio will no longer be attainable; therefore, the flow inside the test section will become unattached. Schlieren images were also taken during this scenario and can be seen in Figures 22 through 25.

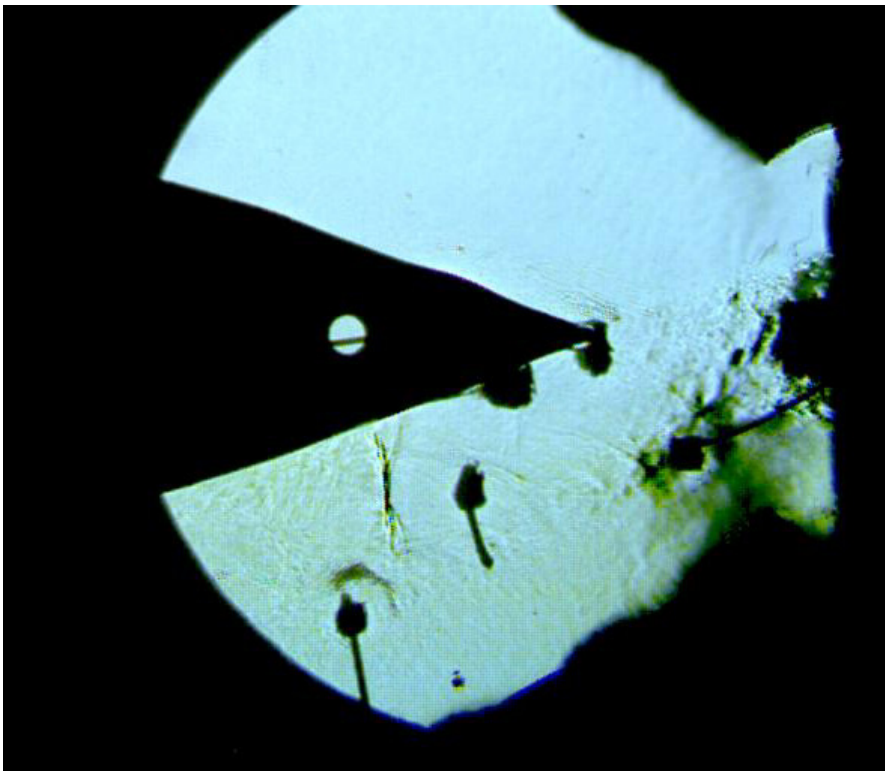

Figure 24 Schlieren Photograph for PRVS of 30u

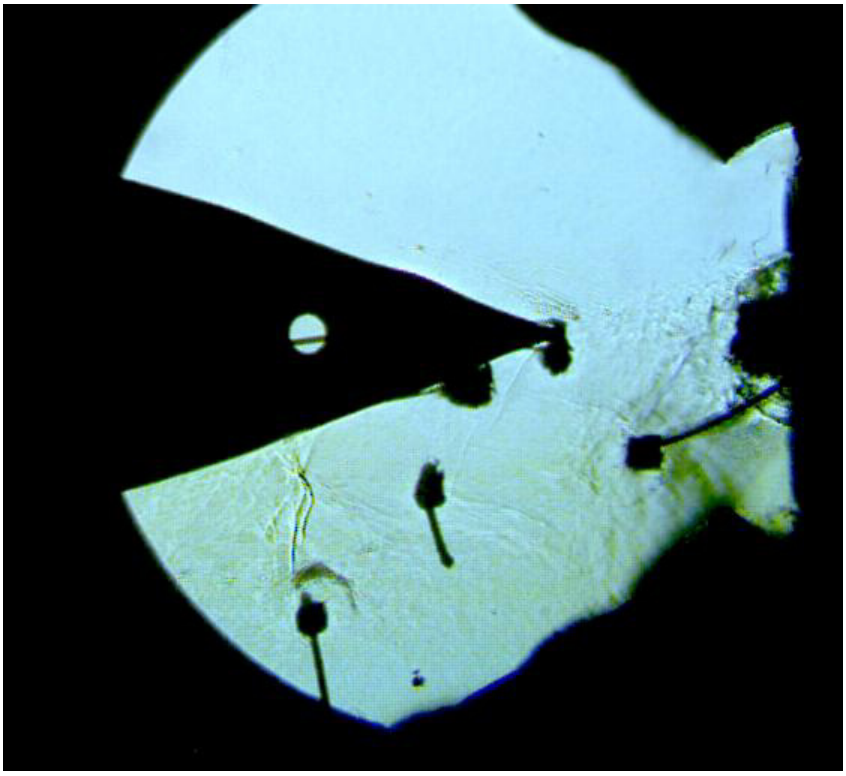

Figure 25 Schlieren Photograph for PRVS of 25u

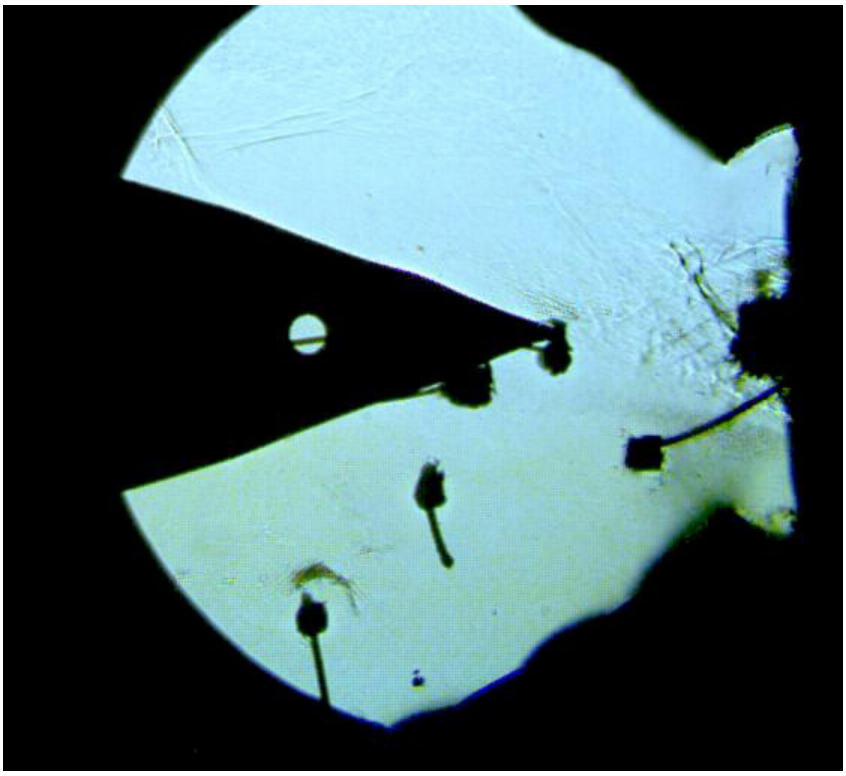

Figure 26 Schlieren Photograph for PRVS of 20u

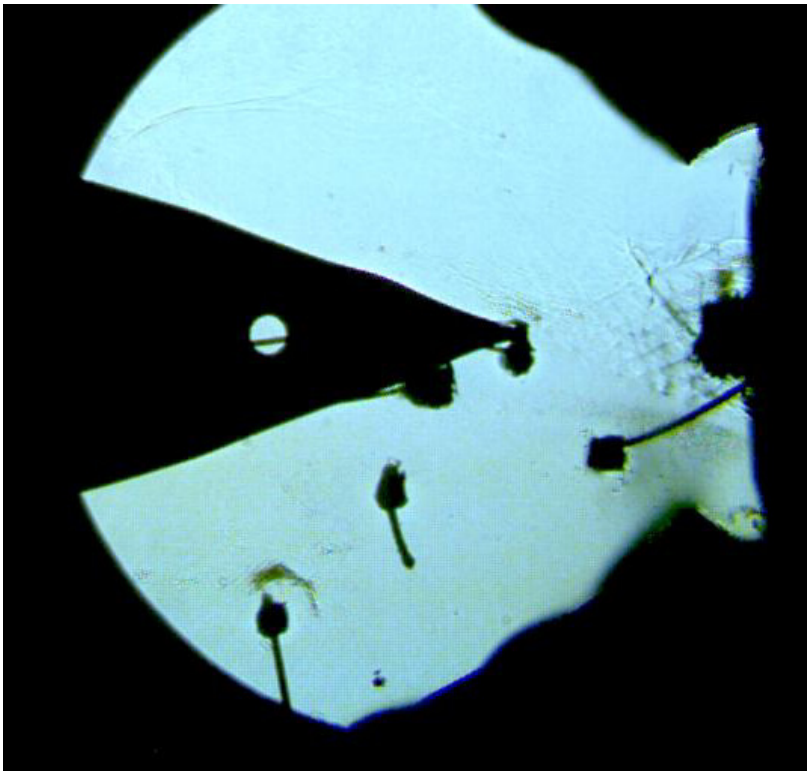

Figure 27 Schlieren Photograph for PRVS of 15u

These images show that while the flow isn't attached it is still supersonic because of the formation of the normal shock wave on one side of the centerbody. Another interesting phenomenon is observed in these images. The flow does not move symmetrically around the centerbody, instead it shifts to one side. What is even more peculiar is that the flow shifts from bottom to top as the PRVS is lowered. Since the only thing changed between runs was the PRVS, the shifting of flow has to be a function of pressure. This flow shifting is most likely due to some nonsymmetry in the nozzle array. This nonsymmetry problem is exacerbated since silicone was used to seal any leaks that couldn't be sealed with gaskets.

V. Conclusions and Recommendations

Conclusions

The first objective to design and fabricate a nozzle array that incorporated the same nozzle geometry as in previous studies, but had a flat exit plane so that interactions between nozzles can be observed. This objective was met by a nozzle array that was flat and could be rotated about its mounting base 360^{O} in 7.5^{O} increments. With this type of apparatus, the nozzle array could be oriented in a way that resembles the previous nozzle array configuration (vertical) and could be rotated to a horizontal position. Thus allowing the user to observe nozzle interactions. The idea for this rotating design was maximizing versatility while minimizing equipment.

The second objective was to investigate the flow field of the new nozzle array using timed based pressure measurements and schlieren photography. This objective was chosen based on the fact that not much was known about the interaction between the shock structure of individual nozzles in this type of nozzle array geometry. Previous studies focused on nozzle geometries that were either a $1/5^{th}$ scale model nozzle rings or a flat array of four nozzles. The first was particularly good at modeling the full scale SBL IFX nozzle array, however shock interactions could not be observed. The later array was only used for loss calculations and rough estimations of shock structure. This objective was accomplished with the use of a basic schlieren set up and a high-speed data acquisition system.

Pressure data collected with the DAS along with the schlieren images gave a clear flow field regime of the optical cavity. With this data, Mach numbers were mapped all throughout the test section. Additionally the schlieren images and pressure data complimented each other,

particularly when determining the Mach number at each pressure transducer location. Flow near the nozzle array exit was found to have a steady state Mach number greater than 2.5 while flow at the exit of the diffuser remained subsonic. These results match those in previous studies very closely.

The schlieren images of the horizontal nozzle array unveiled a vastly complex flow field downstream of the nozzle exit. These images showed that for these tests the nozzles were underexpanded since the jet plumes of each individual nozzle expanded to interact with other expanding jet plumes. Additionally, these images showed that when the vacuum system became saturated by the compressed air system and could only remove incoming air. The oblique shock wave would become unattached from the leading edge of the centerbody but flow would remain supersonic. This supersonic flow would shift up or down based on the PRVS; a phenomenon attributed to nonsymmetry in the nozzle array. Lastly, they showed that the faint radial waves seen in Captain Bergren and Bautista's studies were indeed the intersection of shock and expansion waves.

On a final note, the schlieren images showed the complexity of the jet plume exiting the nozzle array. Unfortunately, the non-uniformity of this flow is not conducive to the lasing process. However, the nozzle array used in this experiment was simply used for viewing shock structure, not for lasing. Because of this, the nozzle array used here was an off-design case; which accounts for the slightly higher shock activity.

Recommendations

The following is a list of recommendations for future studies on this topic. They are listed in order of decreasing precedence.

1. Replace the Plexiglas™ walls of the optical cavity with optical grade quartz glass. This will help schlieren image quality by eliminating distortions due to scratches in the optical cavity.
2. Secondly have a professional drill and place the taps for the pressure transducers. The previous section had holes drilled too big, so silicone was used to fill them up. This led to a severe hindrance in observation into the optical cavity.
3. Install the new DAS. The current Data Acquisition System is very old and slow, in addition to not being connected to the internet. This made getting the pressure data from one computer to another very difficult. The new DAS is based on a LabView program, which can be easily programmed to automatically trigger data collection.
4. It is recommended that this nozzle array be run in positions that are not vertical or horizontal. It may be possible to see other aspects of the nozzle array plume that are not visible in the two positions tested in this study.

Appendix A: Uncertainty Analysis (Bergren, 2002: C-1)

In a previous study, Capt Bergren performed an uncertainty analysis for the instrumentation used to determine the accuracy of a single pressure reading. Originally, this analysis was provided by Wheeler and Ganji (178-182). The calibration list below is broken down by instrumentation component. The Full Scale (FS) for one particular transducer was 50 psia.

Pressure Transducer:

Nonlinearity and hysteresis = ± 0.1% FS

Repeatability = ± 0.1% FS

Thermal sensitivity shift = ± 0.015% FS/^{O}F

Pressure Signal Conditioner:

The calibration errors were categorized into bias ad precision uncertainties. The only bias error in the system due to the pressure transducer was the nonlinearity and hysteresis uncertainties and found to be:

B_1 = 0.1/100 *(50 psia) = ± 0.05 psia

The precision error due to the pressure transducer was from the repeatability and thermal sensitivity shift. To ensure the uncertainty was with a 95% confidence level, the degrees of freedom were assumed to be 30. When referencing a tabulated form of the Student's t-distribution, t = 2. The precision indices could be estimated:

$S_{repeatibility} = S_1 = (0.1\%)(FS)/(100t) = 0.025$psia

$S_{Thermal} = S_2 = (0.015)(T_{shift})(FS)/(100t) = 0.0075$psia where $T_{shift} = \pm 2^{O}$F.

The single uncertainty of the signal conditioner was a bias uncertainty. The error as calculated:

$B_{gain} = B_2 = (\pm 0.5\%)(FS)/100 = 0.25psia$

By combining all the bias and precision errors of the system, a total bias and precision error was calculated:

$B_T = (B_1^2 + B_2^2)^{0.5} = 0.255psia$

$S_T = (S_1^2 + S_2^2)^{0.5} = 0.0261psia$

Finally, the estimated uncertainty for a single pressure reading could be found:

$w_T = (B_T^2 + t\, S_T^2)^{0.5} = 0.261psia = 1793Pa$

Therefore, the uncertainty in a pressure reading was ± 0.3psia (2kPa) with a 95% confidence level considering significant figures.

Calculated Results:

The maximum error in the calculations performed for mass flow and Mach number was investigated considering the uncertainty in pressure. Recall the mass flow equation from equation 1:

$$\dot{m} = \frac{P_t A^*}{\sqrt{T_t}} \sqrt{\frac{\gamma}{R}\left(\frac{2}{\gamma+1}\right)^{\frac{\gamma+1}{\gamma-1}}}$$

Taking the partial derivative with respect to the total pressure, and applying to the nozzle throat:

$$\frac{\partial \dot{m}}{\partial p_t} = \frac{A\sqrt{\gamma}\left(1+\frac{\gamma-1}{2}M^2\right)^{\frac{\gamma+1}{2-2\gamma}}}{\sqrt{RT}}$$

$$w_{\dot{m}} = \frac{\partial \dot{m}}{\partial p_t} w_{pt} = (2.61E\text{-}6)(1793) = 4.7E\text{-}3kg/s$$

The Mach number equation is:

$$M = \frac{\dot{m} RT}{pAa}$$

The sources of error in this equation are due to the mass flow calculation, uncertainty in pressure reading, and temperature fluctuations. The temperature within the test section was assumed to range ± 10^{O}K during the run.

w_T = 10^{O}K

w_p = 1793 Pa

$w_{\dot{m}}$ =4.68E-3kg/s

$\frac{\partial M}{\partial \dot{m}}$=2.97

$\frac{\partial M}{\partial p}$= -3.33E-5

$\frac{\partial M}{\partial T}$=0.0015

To find the maximum error in Mach number:

$$w_M = \frac{\partial M}{\partial \dot{m}} w_{\dot{m}} + \frac{\partial M}{\partial p} w_p + \frac{\partial M}{\partial T} w_T$$

w_M = 0.1

Bibliography

Anderson, John D. Modern Compressible Flow. New York: McGraw-Hill, 1990.

Bautista, Ian. Cold-Flow Testing of a Subscale Model Exhaust System for a Space-Based Laser. Unpublished Thesis. Wright-Patterson Air Force Base, OH: Air Force Institute of Technology, 2003

Bergren, Scott. Fabrication and Cold-Flow Testing of Subscale Space-Based Laser Geometry. Unpublished Thesis. Wright-Patterson Air Force Base, OH: Air Force Institute of Technology, 2002.

Bjurstrom, David R. An Experimental Study of Clustered, Two-Dimensional Rocket Nozzles. Unpublished Thesis. Wright-Patterson Air Force Base, OH: Air Force Institute of Technology, 1984.

Federation of American Scientists. "Space Based Laser (SBL)", 2003. http://www.fas.org/spp/starwars/program/sbl.htm

Kueth, Arnold and Chow, Chuen-Yen. Foundations of Aerodynamics. New York: John Wiley and Sons Inc, 1998

Mattingly, Jack D. Elements of Gas Turbine Propulsion. New York: McGraw-Hill, 1996.

Perram, Glen P. of The Air Force Institute of Technology, Physics Department, Wright-Patterson AFB, OH. "Personal interviews," 2003.

Possel, William H. "Laser Missile Defense: New Concepts for Space-Based and Ground-Based Laser Weapons.", 1998. http://www.fas.org/spp/starwars/program/docs/occppr05.htm

Vita

Ensign David B. Jarrett graduated from Picayune Memorial High School in Picayune, Mississippi. He entered college for undergraduate study at The University of Mississippi in 1998. Upon which time he also entered the Navy ROTC program. In May 2003 Ensign Jarrett graduated Magna Cum Laude with a degree in Mechanical Engineering. Immediately after graduating from Ole Miss, Ensign Jarrett enrolled at the Air Force Institute of Technology. Upon, graduation from AFIT he will attend flight training at Naval Air Station Pensacola, Fl.

REPORT DOCUMENTATION PAGE

Form Approved
OMB No. 074-0188

1. REPORT DATE *(DD-MM-YYYY)*	2. REPORT TYPE	3. DATES COVERED *(From – To)*
04-06-2004	**Master's Thesis**	30 JUNE 03 – 24 MAY 04

4. TITLE AND SUBTITLE

COLD FLOW TESTING OF A MODIFIED SUBSCALE MODEL EXHAUST SYSTEM FOR A SPACE BASED LASER

5a. CONTRACT NUMBER

5b. GRANT NUMBER

5c. PROGRAM ELEMENT NUMBER

6. AUTHOR(S)

JARRETT, DAVID B., Ensign U.S. Navy

5d. PROJECT NUMBER

5e. TASK NUMBER

5f. WORK UNIT NUMBER

7. PERFORMING ORGANIZATION NAMES(S) AND ADDRESS(S)

Air Force Institute of Technology
Graduate School of Engineering and Management (AFIT/EN)
2950 Hobson Way
WPAFB OH 45433-7765

8. PERFORMING ORGANIZATION REPORT NUMBER

AFIT/GAE/ENY/04-J04

9. SPONSORING/MONITORING AGENCY NAME(S) AND ADDRESS(ES)

AFRL/DEBS
Attn: Mr. Dan Marker
3550 Aberdeen Rd. SE
Kirtland AFB NM 87117-5776 DSN: 246-2871

10. SPONSOR/MONITOR'S ACRONYM(S)

11. SPONSOR/MONITOR'S REPORT NUMBER(S)

12. DISTRIBUTION/AVAILABILITY STATEMENT

APPROVED FOR PUBLIC RELEASE; DISTRIBUTION UNLIMITED.

13. SUPPLEMENTARY NOTES

14. ABSTRACT The aim of this research was a continued study of gas-dynamic phenomena that occurred in a set of stacked nozzles as reported by Captains Ian Bautista in 2003 and Scott Bergren in 2002. The arrangement of the stacked nozzles was a modified version of a $1/5^{th}$ scale-model of one quadrant of the conceptual Space Based Laser Integrated Flight Experiment (SBL IFX) gas dynamic laser. Rather than cylindrical rings of nozzles, the stacked nozzles were flat and able to be rotated about a vector normal to the nozzle exits. This set of stacked flat nozzles was installed on a blow-down/vacuum wind tunnel, which in addition to the nozzles, consisted of a stilling chamber, centerbody, supersonic diffuser, and transition structure to join the vacuum and test sections.

The goals of this research were two fold; fist, modify the original scale-model of the stacked cylindrical rings of nozzles so schlieren photography could be used to visualize an average flow field across the nozzles. Secondly, using the schlieren photographs, in conjunction with pressure data, observe the interactions between the individual nozzles. Results have shown that the modified nozzle array produces a vastly complex flow field as well as a highly supersonic flow régime, with Mach numbers that reach as high as 5.6.

15. SUBJECT TERMS

Nozzle Array, Exhaust Manifold, Schlieren Photographs

16. SECURITY CLASSIFICATION OF:			17. LIMITATION OF ABSTRACT	18. NUMBER OF PAGES	19a. NAME OF RESPONSIBLE PERSON
REPORT	ABSTRACT	c. THIS PAGE			Dr. MILTON E. FRANKE
U	U	U	UU	64	19b. TELEPHONE NUMBER *(Include area code)* (937) 255-3636 EX 4720, e-mail: MILTON.FRANKE@afit.edu